Surface-diffusion-driven kinetic growth on one-dimensional substrates

P. I. Tamborenea and S. Das Sarma
Joint Program for Advanced Electronic Materials, Department of Physics, University of Maryland, College Park, Maryland 20742-4111
(Received 2 March 1993)

Motivated by the physics of molecular-beam epitaxial (MBE) growth, we present a detailed numerical study of the dynamic scaling behavior of two atomistic solid-on-solid kinetic growth models in (1+1) dimensions in the presence of surface diffusion under a strong chemical bonding environment. Our goal is to relate stochastic molecular-beam epitaxial growth models with the existing statistical-mechanical-driven dynamical growth models. In the first model, which is the usual stochastic MBE growth model, diffusion of surface atoms follows an Arrhenius activation behavior. The effective growth exponents $\alpha_{\rm eff}$ and $\beta_{\rm eff}$, calculated as functions of the temperature, show a crossover from random deposition ($\beta = 0.5$) to $\beta \approx 0.375$ and $\alpha \approx 1.5$ at intermediate temperatures, and then to $\beta \approx 0$ and $\alpha \approx 0$ at high temperatures. In the second model, which is a manifestly nonequilibrium dynamical model, newly arrived atoms instantaneously migrate to the nearest kink sites, with probability p_1, and within a diffusion length ℓ. After finding a kink site they are allowed to break two bonds and make a nearest-neighbor hop with probability p_2. Here we see a behavior qualitatively similar to that in the first model, but, additionally, for $p_2 \neq 0$, a crossover to the Edwards-Wilkinson universality is observed. Surface morphologies produced by these models are presented with a detailed discussion of the scaling exponents, finite-size effects, and conditions for smooth growth.

PACS number(s): 05.40.+j, 05.70.Ln, 68.35.Fx

I. INTRODUCTION

Nonequilibrium growth dynamics of interfaces, where matter is continuously added to a $(d-1)$-dimensional substrate to drive the interface in the "height" direction, has been an intense area of research activity [1–4] during the past ten years. Part of this interest is technologically motivated because a number of thin-film growth techniques, such as sputtering, chemical vapor deposition, molecular-beam epitaxy (MBE), etc., use far-from-equilibrium deposition methods. But, much of the recent interest in the nonequilibrium interface growth dynamics is fundamental—the problem is a simple example of a self-affine fractal growth process exhibiting generic scale invariance [2] where theoretical techniques of dynamical critical phenomena should be applicable giving us insight into a problem which is manifestly a nonequilibrium statistical mechanical problem. In particular, the universality class of various growth processes and the dynamical morphologies of the evolving surfaces have attracted a great deal of attention. Our goal in this paper is to study in some details the dynamics of a particular atomistic solid-on-solid model of stochastic interface growth where surface diffusion or atomistic hopping in a strong chemical bonding environment plays an essential role. This growth model, which has recently been introduced by Wolf and Villain [5], and by us [6], is inspired by the physics of epitaxial growth where atomistic surface diffusion is known to be a significant kinetic process. We emphasize that all the results presented in this paper are on one-dimensional substrates, and the growth, therefore, is in $d = 1 + 1$ dimensions. (Real MBE growth obviously takes place in $d = 2 + 1$ dimensions.) Our reason for undertaking such a detailed analysis of a particular kinetic growth model is only in part due to its possible connection with experimentally relevant epitaxial growth but mostly due to the fact that this surface-diffusion-driven kinetic model represents a new dynamical growth universality class which has not been anticipated before in the literature, in contrast to other well-known growth universality classes such as the Edwards-Wilkinson [7] (EW) or the Kardar-Parisi-Zhang [8] (KPZ) models which have been exhaustively studied. We feel that a detailed numerical analysis of the one-dimensional (1D) MBE growth model introduced by us [6] and by Wolf and Villain [5] would be useful in putting it in perspective with the existing body of literature on stochastically driven interface growth models. Such a comprehensive numerical analysis of the 1D MBE growth model is our goal in this paper.

According to the dynamic scaling hypothesis [9] of nonequilibrium growth, the width or the root-mean-square fluctuation of the height $W(L,t)$ of a growing interface depends on the system size L and the growth time t according to the scaling relationship

$$W(L,t) = L^{\alpha} f(t/L^{\alpha/\beta}) \tag{1}$$

where f is a scaling function satisfying $f(\infty) \sim$ const and $f(x) \sim x^{\beta}$ for small x. It can be shown that this expression is a consequence of the statistical scale invariance of the growth process [2], which is present if a suitable simultaneous rescaling of length, height, and time (by factors $b > 0$, $b^{-\alpha}$, and $b^{\alpha/\beta}$, respectively) does not alter the statistical properties of the surface fluctuations. According to Eq. (1) and the properties of the function f, for intermediate times $1 \ll t \ll \tau$, where τ ($\sim L^z$ where $z = \alpha/\beta$) is a model-dependent saturation time, the in-

terface width for a fixed substrate size L has a power-law dependence on t,

$$W \sim t^{\beta}, \tag{2}$$

and for $t \gg \tau$, it saturates to a time-independent value $W_{\text{sat}} \equiv W(t \gg \tau)$, which scales with the system size L as

$$W_{\text{sat}} \sim L^{\alpha}. \tag{3}$$

The dynamical critical exponents α and β characterize completely the asymptotic scaling properties of the surface fluctuations of a given growth model and determine its universality class. A number of kinetic growth models have been studied in the light of this scaling hypothesis, and several different universality classes characterized by different sets of values of α and β have been identified.

There have been three alternative types of discrete atomistic simulation-based theoretical approaches to the study of stochastically driven interface growth. The most direct technique has been to use a real-time dynamical simulation, such as molecular dynamics or Monte Carlo method, to study specific systems. Using empirical information for various kinetic parameters and assuming Arrhenius activation behavior for the operative kinetic processes (e.g., surface diffusion as simulated by atomistic hopping and evaporation or desorption), stochastic Monte Carlo simulation within the lattice-gas model has been reasonably successful in quantitatively modeling several aspects of real Si and GaAs MBE growth. While being modestly successful in providing a phenomenological description of real MBE growth, these activated Arrhenius-type stochastic simulations are necessarily limited by small system sizes and simulation times and have not provided much insight into the generic scale invariance or dynamical critical properties of epitaxial growth. These temperature-dependent realistic stochastic simulations suffer from strong finite-size and crossover effects in the critical phenomena sense because the simulation model necessarily involves several competing time scales (or, equivalently, kinetic rates). In addition to the atomistic deposition rate, there are several different hopping rates associated with various diffusion processes (and also a desorption rate if evaporation is important). We will refer to this class of models as stochastic Arrhenius models. The second technique of studying stochastically driven interface growth, aimed specifically at studying the kinetic roughening phenomenon, treats the growth process as a manifestly nonequilibrium phenomenon simulated by random deposition and local atomistic rules for relaxation and incorporation of the deposited particles. The relaxation process is instantaneous and the only time scale in the problem is set by the deposition rate. Eden growth, random deposition with relaxation [10, 11], and ballistic deposition [12, 9, 1] are well-known examples of such discrete growth models. Presumably, the local atomistic rules for deposition, relaxation, and eventual incorporation in these manifestly nonequilibrium simulation models are motivated by the essential kinetic processes governing some real growth phenomenon that one is interested in. We refer to this class of nonequilibrium "toy" models as kinetic growth models. Clearly, kinetic growth models, while catching the essence of a growth process, are less physical than the stochastic Arrhenius simulations. A third class of discrete growth simulation which has also been extensively used employs some microscopic lattice gas Hamiltonian-driven dynamical Monte Carlo simulation to study nonequilibrium growth phenomenon. The single-step model and the restricted solid-on-solid model are examples of this kind of growth simulation. Here the growth simulation itself is not as physically relevant as the other two kinds of simulations discussed above, but the asymptotic critical properties of these models may describe some suitable growth universality class (e.g., the equilibrium and the nonequilibrium versions of the restricted solid-on-solid are known to belong to EW and KPZ universality classes, respectively). In this paper we present numerical results based on the first two types of growth modeling only, and therefore we do not discuss further the last class of models. While the abovementioned discrete atomistic simulations have been useful in elucidating various dynamical aspects of many different specific growth models, an important question from the theoretical perspective has been the viability of constructing continuum differential equations, the classic examples being EW and KPZ equations (Appendix), which correctly describe the coarse-grained large-scale, long-wavelength, long-time, asymptotic behavior of the dynamical evolution of stochastically driven growing interfaces. The goal is to construct continuum equations whose dynamical critical properties are the same as those of the various discrete kinetic growth models so as to establish one-to-one connections between cellular automata-type local atomistic rule-driven growth models and coarse-grained continuum spatiotemporal partial differential equations. We emphasize that, even though several examples currently exist in the literature where one-to-one connections between discrete atomistic growth models and continuum differential equations have been established at least for the dynamical critical properties of the growth model (e.g., Eden model and ballistic deposition are thought to be described by the KPZ equation; random deposition with relaxation model corresponds to the EW equation), we know of no theoretical reason to believe that such a continuum description of atomistic local discrete growth models is always possible. In particular, there may be a subtle problem with the existence of suitable coarse-grained single-valued "height" variables (for which continuum partial differential equations are to be written down) for models with overhangs and vacancies or for models with arbitrarily large kinetic surface roughness. While we will make connections between our discrete atomistic growth simulation results and continuum equations, this is not the main thrust of this paper, partly because the 1D MBE simulation model (a stochastic Arrhenius model) and the related kink diffusion model (a kinetic growth model) whose results we are presenting in this paper seem to correspond (at least, in one substrate dimension) to the continuum linear fourth-order differential equation which was first written down by Herring [13] forty years ago in the context of chemical

potential gradient driven mass diffusion. The issue that we address in some detail is the question of the extent to which the dynamic scaling hypothesis is obeyed by our atomistic simulation results. The EW and the KPZ universality, as discussed in the Appendix, are the linear and nonlinear versions of the appropriate second-order continuum partial differential equations for nonequilibrium growth. Because any other term in the continuum growth equation must necessarily be higher order (in fact, at least fourth order), the asymptotic properties of any growth model must necessarily be dominated by the second-order terms (in fact, by the KPZ nonlinearity) if these second-order terms are actually present in the corresponding growth equation. In particular, assuming the real growth equation to be that given by Eq. (A1) containing all the symmetry-allowed second- and fourth-order terms, the question of crossover becomes significant in the nonasymptotic regime. In fact, in the 1D MBE growth simulation we find clear evidence for a crossover from the kink diffusion universality studied by us (and by Wolf and Villain) to the EW universality at high temperatures when two-bond cutting processes become significant. In our conservative (no desorption, overhang, or vacancy) solid-on-solid (SOS) growth simulation the KPZ nonlinearity is not allowed and, as we have mentioned above, only the linear fourth-order term shows up in our $d = 1 + 1$ simulation. The reason for the absence of the fourth-order nonlinearity in the 1D MBE or the kink diffusion growth model in one substrate dimension is not completely understood yet. (It is possible that this is an extremely slow crossover effect.)

Some of the basic atomistic growth models representing each known universality class and their corresponding continuum models are now briefly described below. (Some details of the continuum description of growth dynamics are provided in the Appendix.)

The random deposition (RD) model consists of particles falling randomly onto the deposit, getting attached to the top of the columns in which they are dropped. The height of the columns follow a Poisson distribution, and therefore $W \sim t^{1/2}$, i.e., $\beta = 1/2$ for all dimensions. Since the different columns grow independently of each other, the surface width never reaches the steady state of saturation, and we can say that $\alpha = \infty$. Pure RD growth involves no correlation between neighboring columns and is therefore unrealistic.

In random deposition with surface relaxation (RDR) [10, 11], particles are randomly dropped onto the surface, but they are allowed to relax within a finite distance, until they find the height minima in the searched areas [see Fig. 1(a)]. Numerical simulations give $\beta = 1/4$ (0) and $\alpha = 1/2$ (0) in $d = 2$ (3) dimensions. The corresponding continuum model is the Edwards-Wilkinson equation [7] [see Appendix, Eq. (A6)].

Ballistic deposition (BD) [12, 9, 1] differs from RD or RDR in the fact that an arriving particle will stick to the deposit at its first encounter with an atom in the deposit within a nearest-neighbor distance [Fig. 1(b)]. That is, the new particle may stick to the side of a high step rather than sliding all the way down to the top of the column randomly assigned to it. In $d = 2$, the numerical simulations indicate $\beta \sim 1/3$ and $\alpha \sim 1/2$, in agreement with the growth equation proposed by Kardar, Parisi, and Zhang [8] [Eq. (A5)]. In $d = 3$, there seems to be numerical agreement between atomistic models and the KPZ equation (Appendix), but the situation is not as well established as for $d = 2$, in part because there are no reliable theoretical estimates of β and α. Many other atomistic models belong to the BD-KPZ universality class, such as the restricted solid-on-solid model of Kim and Kosterlitz [14] and the well-known Eden model.

In contrast to the above three kinetic growth models which have been extensively studied, the kink diffusion (KD) models recently introduced Wolf and Villain [5] and by us [6] have not been studied widely. In these models, particles fall randomly onto the deposit and diffuse within a finite distance to the nearest kink site to maximize [5] or simply increase [6] its local coordination number [Fig. 1(c)]. Simulations in (1+1) dimensions indicate that these models belong to a universality class different from those mentioned above, since the calculated exponents are $\beta \sim 0.375$ and $\alpha \sim 1.3 - 1.4$. These values are very close to the ones obtained with a linear

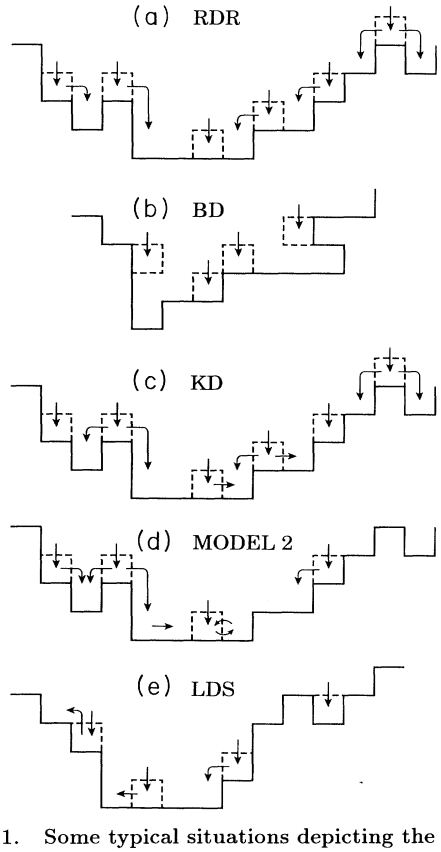

FIG. 1. Some typical situations depicting the rules of deposition and relaxation of atoms in the various kinetic growth models described in the text. (a) Random deposition with relaxation (RDR), (b) ballistic deposition (BD), (c) kink diffusion model (KD), (d) model 2, and (e) Lai–Das Sarma model (LDS). Notice that, in a given model, the arrows represent possible moves of the freshly landed atoms, but the probabilities for those moves are not all the same.

Langevin equation [Eq. (A7)] describing mass diffusion under a chemical potential gradient [13]. In Sec. III we present extensive numerical results for the KD model as defined in Ref. [6], and we also generalize it to allow particles to leave the kink sites by breaking two bonds [model 2, shown in Fig. 1(d) and described in Sec. III]. This generalization provides a more complete connection between the simplified kinetic growth model and the more realistic stochastic Arrhenius 1D MBE model.

Lai and Das Sarma (LDS) [15] have recently introduced a kinetic growth model similar to the KD model, but with the important difference that if an atom falls in a kink site (with an atom underneath and a nearest neighbor on the side) it is allowed to break its two bonds and jump *up or down* [see Fig. 1(e)]. This model belongs to a new universality class, since its exponents are, according to the simulation, $\beta = 0.340 \pm 0.015$ and $\alpha = 1.05 \pm 0.10$, in close agreement with a fourth-order nonlinear growth equation [Eq. (A8)] also analyzed in their paper by renormalization-group techniques. We do not further discuss this model since the LDS nonlinearity does not show up in our simulations.

Very recently [16], Das Sarma and Ghaisas studied a number of kinetic growth models and found evidence that some of their models in (2+1) dimensions realize the universality class of Eq. (A9) with $\nu = 0$ and $\lambda_1 = 0$.

Many numerical studies in relation to the models described above have been done in recent years, especially in the rich universality class of ballistic deposition and the KPZ equation (for references see Ref. [1]). However, few efforts have been made to connect the dynamical scaling theory of these models with realistic growth simulations as carried out by stochastic Arrhenius-type models. Also, the corrections to scaling due to finite-size effects and multiple length and time scales, which may be more relevant to the experimental growth conditions than the asymptotic properties, have not been investigated thoroughly. The goal of this paper is then to study the 1D MBE model and the KD model numerically and understand them as a self-organized dynamical critical phenomenon in some details.

The two growth models studied in this paper employ the square lattice geometry in (1+1) dimensions, and follow the solid-on-solid approximation. The SOS aspect rules out the formation of overhangs and therefore the KPZ equation becomes inapplicable, unless desorption is allowed. We assume desorption to be negligible since it is not a relevant process at the usual MBE growth temperatures. We also mention that the scaling properties of atomistic models are obscured by the fact that in these models there are always typical length scales, other than the system size, such as the interatomic distance, and various diffusion lengths. This complicates the determination of the asymptotic growth exponents since their calculation requires that the system sizes be much larger than all the typical length scales of the model. In computer simulations we are clearly limited in the system sizes that we can study, and therefore we talk about *effective* exponents rather than the asymptotic exponents associated with the models in the thermodynamic limit.

The plan of the rest of this paper is as follows: In Sec. II we introduce and study the stochastic Monte Carlo 1D MBE model (model 1) with Arrhenius activated diffusion. In Sec. III we motivate, define, and study the generalized KD model, or model 2, which is a kinetic growth model inspired by the 1D MBE model. In Sec. IV we give some surface morphologies for the two models in the saturation regime, discuss some aspects of finite-size and crossover effects in our simulations, and provide a discussion of our findings for the critical exponents, making a connection between our two models and the appropriate continuum equations. In Sec. V we speculate about another important issue, i.e., the role of possible nonlinearities in the growth equation corresponding to the KD model. The Appendix contains a discussion of the applicable continuum equation describing the coarse-grained asymptotic properties of stochastically driven interface growth. (We refer to the Appendix appropriately throughout the text of this article.)

II. MODEL 1: A STOCHASTIC ARRHENIUS MODEL

A. Notation and definition

In this section we will discuss dynamic scaling in the 1D MBE model based on an Arrhenius activated surface diffusion. The two-dimensional substrate version of this model has been widely studied in recent years [17] and it is the accepted model for stochastic MBE simulation since it reproduces well the growth characteristics observed experimentally. As a first step in the study of the dynamic scaling properties of MBE growth, which in practice takes place in three dimensions, in this paper we will limit ourselves to two-dimensional growth. The height of the deposit at the ith substrate site is denoted by h_i and the width of the one-dimensional growing interface is defined as the root mean square of the height, i.e.,

$$W(L,t) = \left[\frac{1}{L} \sum_{i=1}^{L} (h_i - \bar{h})^2 \right]^{1/2} . \tag{4}$$

To obtain good statistics, the width squared (W^2) is averaged over many runs, usually around 1000 and 100, for small and large systems.

There are three kinetic processes in our model 1: random deposition of atoms onto the deposit (we take the deposition rate to be $R_d = 1$, that is, one atom per site per second, or one monolayer per second), and two kinds of hopping, or diffusion, where one and two bonds are broken via thermally activated diffusion, respectively. After breaking its bonds, the atom hops to one of its neighboring columns, provided that the initial site is as high as or higher than the final one. We are using a solid-on-solid approximation and therefore we do not allow vacancies and overhangs. The relevance of this approximation will be discussed later in the context of the analysis of the surface morphologies produced by our simulation. The diffusion rates follow an Arrhenius behavior characterized by a configuration-dependent activation energy given by

$$R_n = R_0 \exp[-E_A(n)/k_BT]. \quad (5)$$

Here $R_0 = 2k_BT/h$ is a diffusion prefactor which depends weakly on the temperature T, and k_B and h are the Boltzmann and Planck constants, respectively. $E_A(n) = E_0 + nE_B$ is the site-dependent activation energy, where E_0 is the activation energy of a free atom, E_B is the binding energy per bond, and n is the number of nearest neighbors that the atom has in its initial site. In our case an atom can hop only when n is 1 or 2, $n = 1$ corresponding to the situation where the atom has initially only a neighbor underneath, and $n = 2$ implies a nearest-neighbor underneath and another on the side. Thus R_1 and R_2 correspond respectively to one bond- and two bond-breaking hopping rates. The values of the activation energies, $E_0 = 1$ eV, and $E_B = 0.3$ eV are chosen with Si and GaAs in mind, but they are only semiquantitatively correct. (Note that the activation barrier for the "vertical" and the "lateral" bonds are 1.3 and 0.3 eV, respectively.)

We note that at low temperatures, $R_1 \ll R_d$ (note that $R_2 \ll R_1$ always), and therefore we expect strong crossover effects arising from random deposition. On the other hand, when $R_1 \gg R_d$, the diffusion length is long and finite-size effects dominate. It is only when $R_1 \sim R_d$ that we expect to see a nontrivial growth universality. It is important to notice that the diffusion rates depend exponentially on the temperature and therefore vary greatly as we span a temperature range of a few hundred degrees. The dependence on the number of bonds or the coordination number is also exponential, and this produces a large difference in the respective rates R_1 and R_2 of one-bond and two-bond breaking events. To illustrate this point, we give here a few values of the diffusion rates: at the temperatures 400, 500, 600, and 700 K, R_1 (R_2) takes the values 6.7×10^{-4} ($1. \times 10^{-7}$), 1.58 (0.001), 288.8 (0.87), and 12 233 (84.4), respectively. Since $R_1 \gg R_2$, the atoms tend to spend most of the time in kink sites, especially at high temperatures. This observation, in fact, motivated us to construct our KD kinetic growth model (discussed in Sec. III), where the deposited atoms instantaneously relax to the local kink sites (and stay there forever) as the nonequilibrium version of the 1D MBE model. We also note that three-bonded ($n = 3$) sites are essentially stable in our simulation and are always at the local height minima. Thus diffusion to the three-bonded sites is qualitatively similar to the relaxation to the local height minima in the RDR kinetic growth model.

B. Calculating exponents α and β

We calculate the critical exponents α and β from the dependence of the interface width W on the growth time t and the system size L, as given in Eqs. (2) and (3). In Fig. 2 we show log-log plots of W versus t in model 1, for $T = 500$ and 600 K, and for various system sizes. Here we can see the different regions predicted by the scaling hypothesis: for very early times (before the first layer is completed), there is a power-law dependence corresponding to random deposition ($\beta = 1/2$); for intermediate

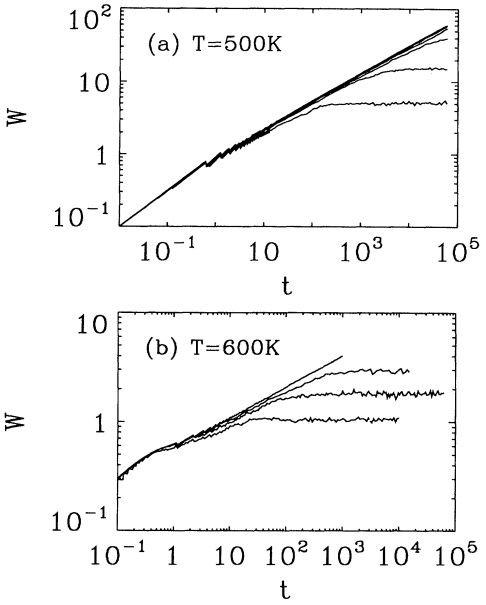

FIG. 2. The calculated interface width W as a function of growth time t in model 1: (a) $T = 500$ K, from bottom to top: $L = 8, 16, 32, 64, 128, 256, 1024$ (for the smaller system sizes we averaged over 500 runs and for $L = 1024$ over 32 runs); (b) $T = 600$ K, $L = 32,64,128,16\,384$ (averaged over 300, 128, 128, and 50 runs, respectively).

times, the scaling law $W \sim t^\beta$ is obeyed, with β having the characteristic value of our particular model; finally, at long times, saturation is reached, and the width stops increasing. In Fig. 2(a), where $T = 500$ K, only for small system sizes up to $L = 64$ can we see the saturation effect within the time scale of our simulation (65 536 layers). At $T = 600$ K [Fig. 2(b)], the onset of saturation for $L = 32$ occurs almost four decades earlier than at 500 K, and we can see the saturation regime for much larger values of L within a given growth duration. This is due to the much faster diffusion at 600 K (compared with 500 K) arising from activated hopping.

Note that for the small system sizes at $T = 600$ K [Fig. 2(b)], the time window where the scaling law $W \sim t^\beta$ holds practically disappears because of the early saturation produced by the relatively large (compared to the system size) diffusion length. This is an extreme situation showing that the exponents calculated in a finite-size simulation are not the asymptotic ones corresponding to the thermodynamic limit $L \to \infty$. Therefore, throughout this paper we will be reporting on our calculated values of the *effective* exponents, which are usually close to the asymptotic values only if the characteristic lengths of the model (diffusion lengths) are small compared with the system size. In Fig. 3 we see that as the t^β time window shrinks, the effective exponent β_{eff} becomes lower than the asymptotic $L \to \infty$ value due to strong finite size effects. Figure 3(a) shows the calculated *effective* exponent β_{eff} in model 1 as a function of the temperature. We give results for $L = 256, 512$, and 1024, obtained from curves of $\log_{10} W$ versus $\log_{10} t$,

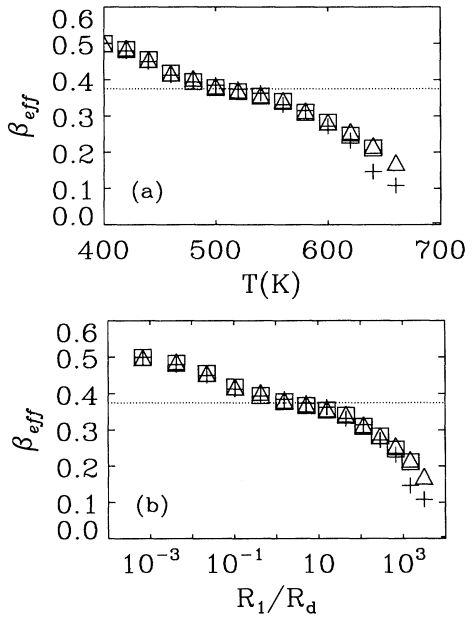

FIG. 3. The calculated *effective* exponent β_{eff} in model 1, as a function of (a) the temperature T and (b) the ratio R_1/R_d (the temperature T defines the hopping rate R_1 via an Arrhenius rule; we have $R_1 \approx R_d$ for $T \approx 500$ K for the parameters used). The different symbols correspond to different system sizes: crosses, $L = 256$; triangles, $L = 512$; and squares, $L = 1024$. (Data averaged over 128 runs except for $T = 600$ K where 256 runs have been used.) The dotted line corresponds to $\beta = 0.375$.

with growth duration of 1000 layers, and typically averaged over 128 independent runs. In Fig. 3(b) we present the same results but as a function of R_1/R_d, the ratio of the fastest diffusion rate and the deposition rate, given in number of atoms deposited per site per second.

In the limit $T \to 0$ (or $R_1/R_d \to 0$), we are, clearly, in the random deposition case, and the height of the deposit follows a Poisson distribution, with $\beta = 1/2$ (since in this case there are no correlations between the different columns, there is no saturation, and the roughness increases without limit even in a finite system. Thus we can say that $\alpha = \infty$).

At low temperatures (small R_1/R_d), we see that β_{eff} is very close to the random deposition value $\beta = 1/2$, which we interpret as a finite-time effect, because the relatively weak diffusion mechanisms cannot give rise to correlations among the different columns in the limited time of the simulated growth.

As we increase the temperature, β_{eff} decreases and shows a plateau at a value close to 0.375 [dotted line in Figs. 3(a) and 3(b)], around $T \approx 500$ K ($R_1/R_d \approx 1$). This plateau at 0.375 is the first piece of evidence that leads us to believe that, at intermediate temperatures, 1D MBE belongs to a universality class different from those represented by the EW and the KPZ models, i.e., the KD model, which was introduced in Refs. [5, 6]. The existence of this new universality class and the fact that model 1 belongs to it (at least) in a limited temperature range will become clearer in the next section, where we study the KD model in which the atoms are allowed to relax to kink sites and stay there forever. Therefore, in Figs. 3(a) and 3(b) we see a crossover between RD and a new universality class (KD) with $\beta = 3/8$.

At higher temperatures ($R_1/R_d \gg 1$), β_{eff} keeps decreasing and eventually tends to zero in the high-temperature limit. There are two distinct reasons for β_{eff} to decrease from the asymptotic KD value with increasing temperature. Since high temperatures produce long diffusion lengths, this decrease in β_{eff} is in part a pure *finite-size* effect. (Note that at $T > 600$ K, β_{eff} for $L = 256$ is smaller than for the other two larger system sizes.) On the other hand, at high temperatures, the rate R_2 becomes important, and the possibility of breaking two bonds gives the atoms some chance to minimize their local heights rather than simply maximizing the coordination number. This new mechanism that allows the atoms to migrate to nearby local height minima by breaking two bonds should produce a crossover from the KD to the RDR universality as the rate R_2 increases with increasing T. Since there is no evidence of a plateau at $\beta = 0.25$ in the curve of β_{eff} versus temperature of Fig. 3, we support this conjecture by presenting, in Sec. III, results for a generalized version of the KD model, where the arriving atoms first look for a kink site and afterwards they are allowed to break the bonds and move further, with a certain probability. We will see that this model crosses over from the KD to the RDR universality, which leads us to believe that in the thermodynamic limit ($L \to \infty$), at high temperatures, the model 1 would also produce the EW exponents $\beta = 1/4$ and $\alpha = 1/2$.

Figures 4(a) and 4(b) show the dependence of the effective roughness exponent α_{eff} on the temperature T and the ratio R_1/R_d, respectively. The method used to determine the exponents $\alpha_{\text{eff}}(T)$ is illustrated in Figs. 4(c) and 4(d). For a given temperature, we let the growth time be long enough so that saturation is reached for systems of sizes L =20, 25, and 30. Since we are assuming that W_{sat} scales as $W_{\text{sat}} \sim L^{\alpha_{\text{eff}}}$, we then obtain the exponent α_{eff} using a linear fitting of $\ln(W_{\text{sat}})$ versus $\ln(L)$ [Fig. 4(d)]. Notice that the values of the effective exponents α_{eff} given in Figs. 4(a) and 4(b) have been obtained using the same set of system sizes ($L = 20, 25, 30$) for the different temperatures, in the spirit of Fig. 3, where the exponent β_{eff} is given as a function of T (and R_1/R_d) for three *fixed* values of L. As it happened in that case, the finite-size effects will be more important at high temperatures, where the diffusion lengths are longer. Notice that to obtain α_{eff} we need growth durations larger than the saturation time τ, which is of the order of $\tau \sim L^{\alpha/\beta} \approx L^4$. This time is extremely large for large systems, making it very difficult to evaluate the "asymptotic" values of α [in other growth models, $z = \alpha/\beta$ is usually smaller than 4, which makes the calculation of α easier; for example, for ballistic deposition, $z = \alpha/\beta = 1.5$ in (1+1) dimensions].

As we pointed out above, as $T \to 0$, model 1 approaches the RD model, which does not undergo saturation of the interface width at long times, since the different columns of the aggregate are uncorrelated. The deter-

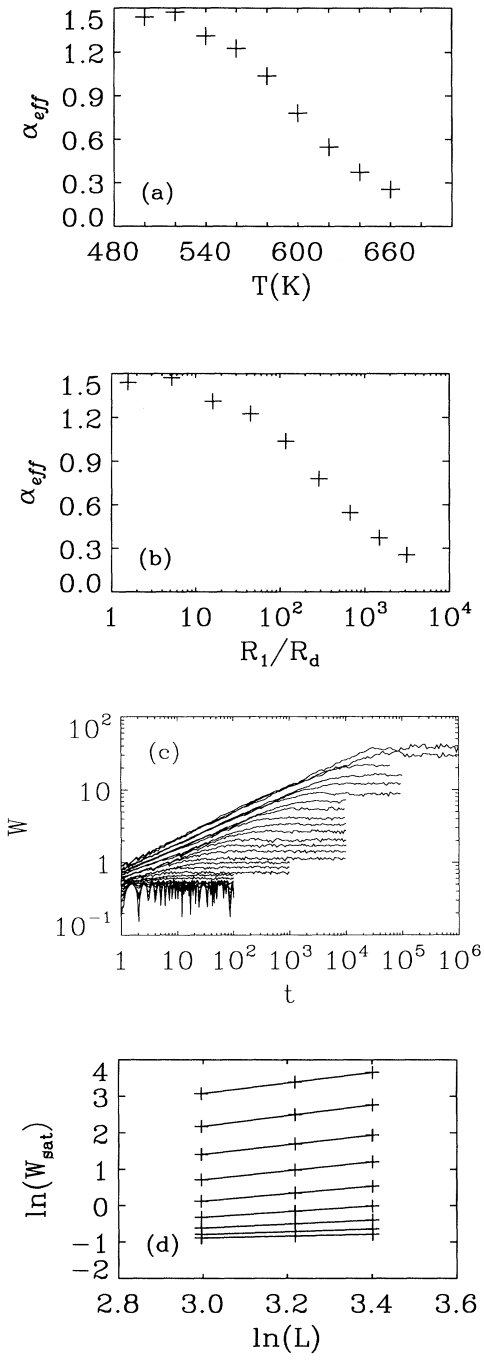

FIG. 4. (a) The calculated *effective* exponent α_{eff} as a function of the temperature T in model 1; (b) α_{eff} as a function of the ratio R_1/R_d; (c) interface width W as a function of time t. The saturation regime data from these curves were used to obtain α_{eff}. From top to bottom, groups of three curves correspond to the system sizes $L = 30, 25, 20$ for the temperatures $T = 500, 520, \ldots, 640$ K (data averaged over 500 runs for temperatures lower than 600 K and over 1000 for $T \geq 600$ K). (d) Logarithm of the saturation width as a function of the logarithm of the system size. For each temperature, three points and their least-squares fit are given, obtained from the curves shown in (c). The slopes of the fits are the effective exponents α_{eff}.

mination of the exponent α in our model at low temperatures therefore becomes practically impossible because the onset of saturation occurs at very long growth times. This is the reason why the lowest temperature considered in Fig. 4(a) is 500 K, where it was necessary to grow 10^6 atomic monolayers to see the saturation regime clearly. At $T = 500$ K we have $\alpha_{\text{eff}} \approx 1.45$, and for higher temperatures the finite-size effects combined with the crossover to RDR cause the effective exponent α_{eff} to decrease, down to $\alpha_{\text{eff}} \approx 0.77$ for $T = 600$ K. Notice that in the range of temperatures where the hopping rate $R_1 \approx 1$ (around $T \approx 500$ K), where we expect the finite-time and finite-size effects to be weakest, we obtain $\beta_{\text{eff}} \approx 0.375$ [Fig. 3(a)] and $\alpha_{\text{eff}} \approx 1.45$ [Fig. 4(a)], in agreement with the exponents corresponding to the linear fourth-order Eq. (A7).

C. Scaling

According to the dynamic scaling hypothesis of Eq. (1), for each growth model there exists a unique function f such that

$$f(t/L^z) = W(L,t)/L^\alpha, \tag{6}$$

satisfying $f(\infty) = \text{const}$, and $f(x) \sim x^\beta$ for small x, where $z = \alpha/\beta$. In Fig. 5(a) we plot $W(L,t)/L^{\alpha_{\text{eff}}}$ as a function of $t/L^{z_{\text{eff}}}$ and see the scaling collapse of data for the model 1 for different system sizes, for $T = 500$ K. In Fig. 5(b) we show results for $T = 600$ K. Notice

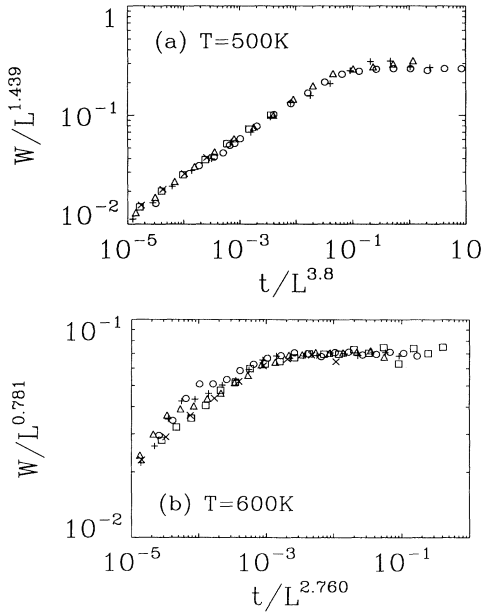

FIG. 5. Scaling function $f(t/L^{\alpha_{\text{eff}}/\beta_{\text{eff}}}) = W/L^{\alpha_{\text{eff}}}$ as obtained from the simulation in model 1. The figure shows the collapse of the data into the scaling function form for different system sizes: (a) $T = 500$ K, $L = 10$ (circles), 25 (pluses), 30 (triangles), 64 (squares), and 128 (crosses); (b) $T = 600$ K, $L = 20$ (circles), 25 (pluses), 30 (triangles), 64 (squares), and 128 (crosses).

that the effective exponents by which we rescale the time and the width are different for different temperatures and therefore the existence of a unique (for all values of T) scaling function is not explicitly verified. This is consistent with our expectation of a crossover from the KD to the RDR universality and also with the fact that our exponents are affected by finite-size effects. Although the growth exponents and the scaling function are affected by crossover and finite-size effects, we verify that *at a given temperature* the rescaled width-versus-time data always collapse to a unique functional form. This collapse is in part a trivial consequence of the way the effective exponents have been calculated, but it does demonstrate that the saturation time has the form $\tau = AL^z$, with A an L independent constant.

D. Simulation without two-bond-breaking hops

We also studied a variation of the original model 1, putting $R_2 = 0$ explicitly, i.e., where two-bond-breaking hops are forbidden, and therefore the only diffusion mechanism is one-bond-breaking nearest-neighbor hops. This implies that atoms in kink sites will remain there forever. With this modification the model becomes equivalent to the kinetic KD model and a high-temperature crossover to EW universality is not expected anymore. In Fig. 6(a) we show the effective exponent β_{eff} as a function of the substrate temperature T. Again we see the crossover from the RD to the KD universality at low temperatures, but the important difference with the $R_2 \neq 0$ case is that the plateau at $\beta = 0.375$ is more pronounced due to the fact that there is no crossover to the RDR-EW universality ($\beta = 0.25$) in the current situation. Notice that at high temperatures β_{eff} decreases somewhat as expected due to the finite size of the system, but this decrease is not nearly as strong as in the case of the original simulation (Fig. 3). We conclude that the strong finite-size effect observed in Fig. 3 responsible for β_{eff} going rapidly to zero comes mostly from the diffusion associated with the breaking of two bonds. In Fig. 6(b) we show the width W as a function of time t, used to calculate β_{eff} versus T given in Fig. 6(a). Each curve corresponds to a different temperature, and β_{eff} is obtained from the last decade of each curve.

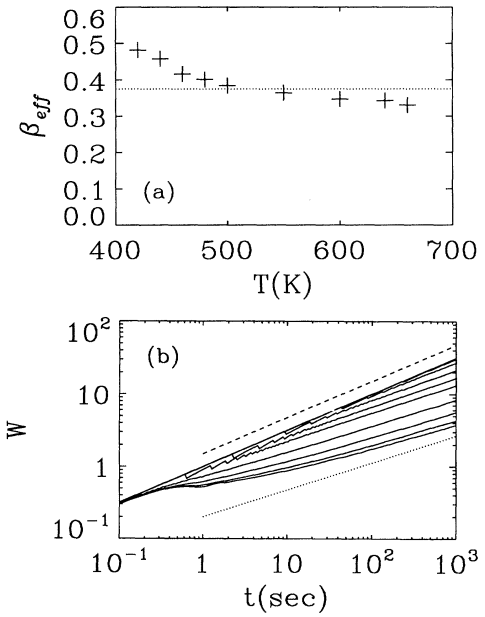

FIG. 6. Simulation results for model 1 with the two-bond-breaking hopping rate $R_2 = 0$. (a) Effective exponent β_{eff} as a function of the temperature; (b) the width W as a function of time t, used to calculate β_{eff} given in (a). The system size used is $L = 1000$, and curves from top to bottom correspond to increasing temperature. The effective exponents are calculated from the slope of the curves in the highest decade.

III. MODEL 2: A KINETIC GROWTH MODEL

A. Notation and definition

The simulation results discussed in the preceding section suggest that the realistic (in the sense that the diffusion rates follow an Arrhenius activation behavior) model 1 crosses over from random deposition (at $T = 0$ K) to a new universality class (at intermediate $T \sim 500$ K), and then (we conjectured, but strong finite-size effects prevent us from obtaining the corresponding values for the growth exponents) possibly to the EW universality class (as the two-bond-breaking hopping rate R_2 becomes important at higher temperatures). In finite-size systems, increasing the temperature further leads to a completely smooth surface, and therefore the growth exponents tend to zero as $T \to \infty$. This "smooth" growth is just a result of the effective diffusion length becoming larger than the simulation system size.

Therefore, the study of the scaling exponents for model 1 brings up the following questions.

(i) Is there really a new universality class with $\beta = 3/8$ and $\alpha \simeq 1.4$?

(ii) Which mechanism of model 1 is relevant in producing these new exponents?

(iii) Does model 1 cross over to RDR with EW universality when R_2 becomes large?

To answer these questions we introduce a simplified kinetic growth model, which we call model 2, that preserves many aspects of model 1 but gives us more freedom to control the diffusion mechanisms and thereby study their effects on the scaling exponents. Our model 2 is a generalization of the model defined in Ref. [6], which we call kink diffusion model. The KD model constitutes a possible description of MBE at intermediate temperatures, where diffusion to kink sites is the most important surface relaxation mechanism. It was pointed out in Refs. [6, 5] that, according to the simulations, the KD model belongs to a universality class different from RD-EW and BD-KPZ. In this section we present more complete numerical evidence for this and generalize the KD model to include the possibility for the atoms to break two bonds and leave the kink sites. This process changes the universality class from KD to RDR, as we will see below.

Model 2 preserves the square lattice geometry and the

solid-on-solid aspect of model 1, but, being a kinetic growth model, the diffusion rates are eliminated by letting the atoms diffuse only once when they are being incorporated to the deposit. The incorporation of new atoms is done in the following steps [see Fig. 1(d)].

Step 1: The atom lands initially on a randomly chosen column.

Step 2: The atom relaxes instantaneously to the *nearest kink site* (a site with 2 or 3 nearest neighboring atoms) with probability p_1, provided that the kink is within a distance ℓ ($0 < \ell \ll L$, where L is the lateral system size) of the initial deposition site, and that it does not have to jump upwards to reach the kink.

Step 3: If the atom finds a site with two nearest neighbors, there is a probability p_2 that it will break the two bonds and hop to the next column (again, the atom is not allowed to move up).

Model 2 differs crucially from model 1 in the fact that the atoms are allowed to relax only once (when they are being deposited) and not continuously, and therefore we are left with only one rate in the problem, namely the deposition rate. However, we incorporate in model 2 diffusion mechanisms which are analogous to the ones operating in model 1. Step 2 corresponds to the hopping involving breaking one bond, which makes the atom hop around until it finds a kink site. The rate R_1 of the old model corresponds now to the parameters p_1 and ℓ. Step 3 is related to the two-bond-breaking hops of the former model, the probability p_2 playing a role similar to the hopping rate R_2.

B. Simulations with $p_2 = 0$

If we let $p_2 = 0$ (no two-bond-breaking hops) model 2 reduces to the KD model introduced in Ref. [6]. First we present more complete numerical results for this case, including our calculations of the roughness exponents α, which we mentioned only briefly in Ref. [6].

In Figs. 7(a) and 7(b) we show some log-log plots of W as a function of growth time t in model 2, with $p_2 = 0$, for various values of ℓ and L. We verify in these plots that model 2 satisfies the scaling hypothesis $W \sim t^{\beta}$, for intermediate times, and that the correlations between different columns introduced by the migration of new atoms to kink sites result in saturation of the width W at long times. The curves for the small system sizes show the saturation regime from which α is calculated, and the curve for $L = 1000$ follows over a wide time interval the power law $W \sim t^{\beta}$, used to calculate β.

In Fig. 8(a) we show our calculated values of β_{eff} as a function of p_1 for model 2, with $p_2 = 0$, for various values of the diffusion length ℓ. We can see that the finite-size effects are much less important here than in model 1, and it seems clear that $\beta \approx 0.375$, *independent of* p_1, which implies that our second growth model (when $p_2 = 0$) belongs to a universality class other than EW and KPZ universality classes. Only for small values of p_1 does β_{eff} depart from the value 0.375 and approach 0.5, but this is clearly due to the crossover to RD as $p_1 \to 0$. In Fig. 8(b) we show a log-log plot of W as a function of growth time

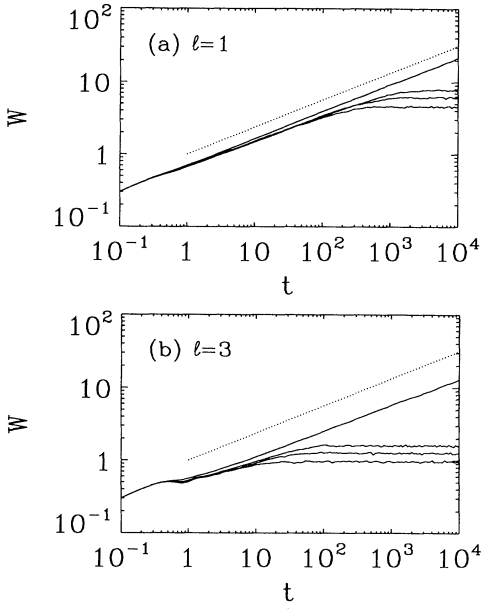

FIG. 7. The calculated width W as a function of the growth time t in model 2 for $p_1 = 1$, $p_2 = 0$, $L = 30, 40, 50, 1000$ (averaged over 1000 runs for $L = 30, 40, 50$ and over 100 runs for $L = 1000$), and (a) $\ell = 1$, (b) $\ell = 3$. The dotted line corresponds to $\beta = 0.375$.

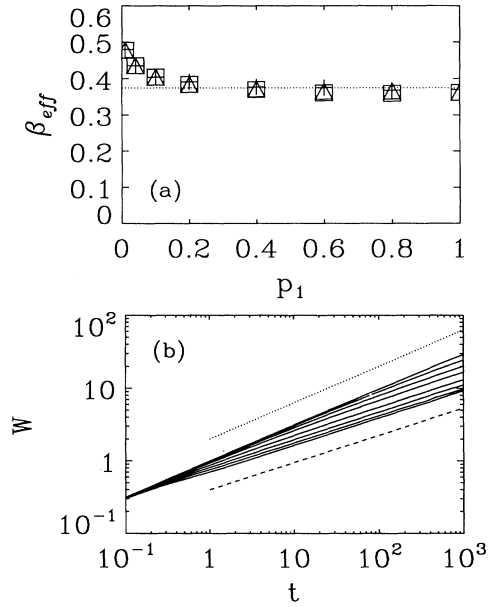

FIG. 8. Simulation results for model 2 with $p_2 = 0$. (a) The calculated effective exponent β_{eff} as a function of the diffusion probability p_1. The different symbols indicate different diffusion lengths: pluses, triangles, and squares correspond to $\ell = 1$, 2, and 3 respectively. (b) The calculated width W as a function of growth time t, for various values of p_1 (from top to bottom $p_1 = 0.01, 0.04, 0.1, 0.2, 0.4, 0.6, 0.8, 1$) and $\ell = 1$. The system size is $L = 1000$ and results are averaged over 100 runs. The dotted line corresponds to $\beta = 0.5$ and the dashed line to $\beta = 0.375$. These are the curves of W vs t from which the effective exponents β_{eff} for $\ell = 1$ shown in (a) are calculated. The effective exponents are the slope of the curves in the highest decade.

t for $L = 1000$, $\ell = 1$, and various values of p_1. For $p_1 = 0.01$ we observe that the finite-time effect produces a high slope, close to $\beta = 0.5$, corresponding to RD. As we increase p_1, the slopes of the curves decrease rapidly, leading to $\beta \approx 0.375$, the characteristic value of β for this model, as shown in Fig. 8(a).

It is interesting to determine how the effective exponent β_{eff} that we obtain with our necessarily finite-size simulation depends on the diffusion length given by the parameter ℓ. In Fig. 9(a) we plot β_{eff} as a function of ℓ, for $p_2 = 0$ and $p_1 = 1$. As the diffusion length increases the effective exponent decreases somewhat due to finite-size effects. However, it seems clear that β will not depend on ℓ in the thermodynamic limit ($L \to \infty$) or, in other words, $\beta \approx 3/8$, for our model, *independent of* ℓ. In Fig. 9(b) we show the curves of the width W as a function of time t employed to calculate β_{eff}. Since β_{eff} is least affected by finite-size effects when $\ell = 1$ and by finite-time effects when $p_1 = 1$, we made additional simulations for $\ell = 1$ and $p_1 = 1$ and system sizes $L = 10^5$ and 10^6 to determine our best estimate of the asymptotic exponent β for model 2 with $p_2 = 0$. The result is $\beta_{\text{eff}} = 0.371 \pm 0.005$.

The effective exponent α_{eff} as a function of the diffusion length ℓ in model 2, for $p_2 = 0$, is shown in Fig. 10(a). In Fig. 10(b) we show the interface width W as a function of time t for some values of the diffusion length ℓ. Figure 10(c) is a plot of $\ln(W)$ versus $\ln(L)$ for ℓ from 1 to 9. For consistency, we calculated α_{eff} using the saturation widths for the same set of system sizes for all values of ℓ (i.e., $L = 30, 40, 50$). From Fig. 10(a) we see that for small ℓ, α_{eff} is around 1.3 and decreases as ℓ increases. Analogously to what happened in model 1, for large diffusion lengths, the finite-size effects decrease our effective exponent α_{eff} [notice that the saturation widths W used to calculate α_{eff} in Fig. 10(c) for large ℓ are very small and therefore the calculated effective exponent α_{eff} will be far from the asymptotic value]. Using system sizes larger than the ones used in Fig. 10, namely, $L = 40, 80$, and 160 (the W versus t curves for these runs are shown in Fig. 11), our best estimate of the asymptotic value of α turns out to be $\alpha = 1.32 \pm 0.04$.

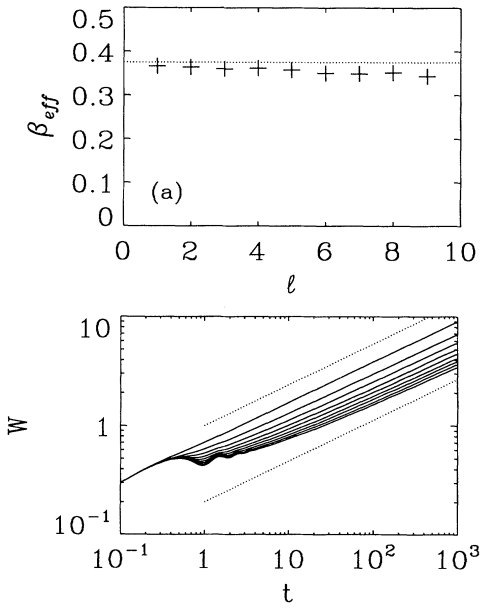

FIG. 9. (a) The calculated effective exponent β_{eff} as a function of the diffusion length ℓ in model 2, for $p_1 = 1$ and $p_2 = 0$. The dotted line corresponds to $\beta = 0.375$. (b) The calculated width W as a function of growth time t, for various values of ℓ (curves from top to bottom correspond to increasing ℓ), used to calculate β_{eff} given in (a). The system size $L = 10\,000$ and the number of runs is 100. The effective exponents are the slope of the curves in the highest decade.

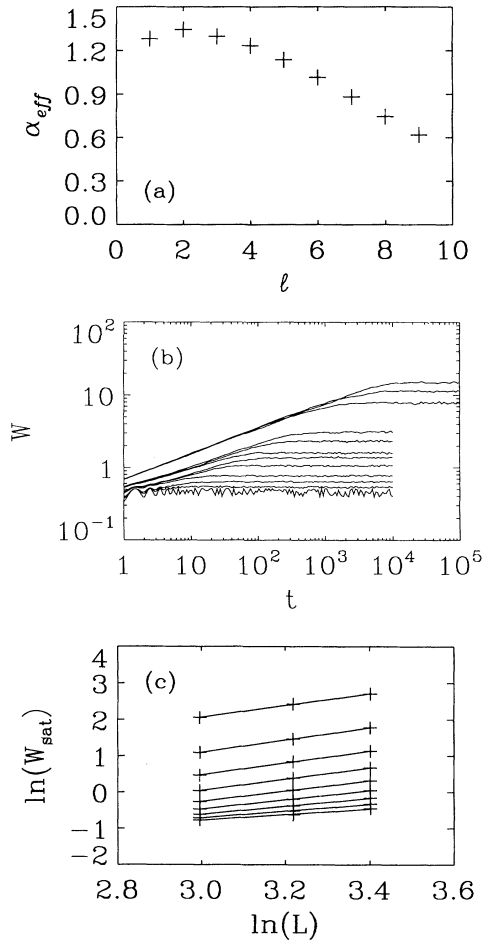

FIG. 10. (a) The calculated effective exponent α_{eff} as a function of the diffusion length ℓ in model 2, for $p_1 = 1$ and $p_2 = 0$. (b) Interface width W as a function of time t. The saturation regime data from curves like these were used to obtain α_{eff}. From top to bottom, groups of three curves correspond to the system sizes $L = 50,40,30$ for the diffusion lengths $\ell = 1$, 3, 5, and 9. Results are averaged over 1000 runs. (c) Logarithm of the saturation width W_{sat} vs logarithm of the system size L, for different diffusion lengths ℓ. The straight lines are linear fits to the calculated saturation widths, and their slopes are the effective exponents α_{eff}. From top to bottom, the curves correspond to ℓ from 1 to 9.

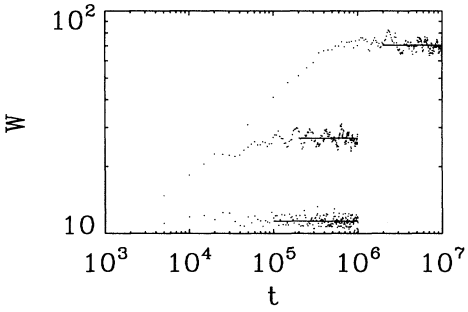

FIG. 11. Interface width W as a function of time t in model 2 for $\ell = 1$, $p_1 = 1$, and $p_2 = 0$. These simulation results were used to obtain our best estimate of the asymptotic exponent α. From bottom to top, the curves correspond to the system sizes $L = 40$, 80, and 160. Results are averaged over 60, 100, and 100 runs, respectively. The straight lines on the saturated width regions give the average values of $W_{\rm sat}$ for each system size.

C. Simulation with $p_2 \neq 0$

We now show results for model 2 when the probability p_2 of breaking two bonds is nonzero. The motivation of this analysis is to provide evidence that the model 1 will crossover to EW-RDR at high temperatures, because in that regime the rate of hops involving breaking of two bonds becomes important, and therefore the atoms will have a chance to leave the kink sites and jump down, minimizing their height.

In Fig. 12 we show some curves of the width W as a function of the time t, in model 2, for $p_1 = 1$, $p_2 = 1$, and $\ell = 1$. We see the saturation regime for small L; the slope close to 0.25 for $L = 10\,000$ indicates that this model is in the universality class of RDR.

In Fig. 13(a) we show $\beta_{\rm eff}$ as a function of p_2 and in Fig. 13(b) the curves of W versus t used to calculate $\beta_{\rm eff}$. We clearly see the crossover from the KD universality class with $\beta = 0.375$ to the RDR universality class with $\beta = 0.25$. In Fig. 14(a) we show the effective exponents $\alpha_{\rm eff}$ as a function of the probability p_2, for $\ell = 1$ and

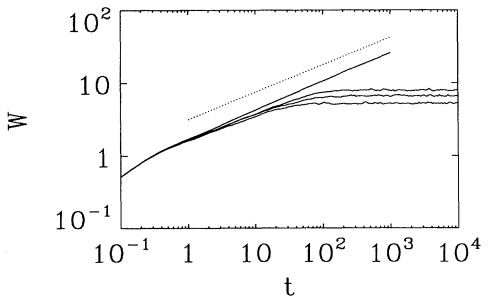

FIG. 12. The calculated width W as a function of growth time t in model 2, for $p_1 = 1$, $p_2 = 1$, and $\ell = 1$. The different curves correspond to different system sizes: from bottom to top $L = 30, 40, 50$, and 10 000. Results are averaged over 1000 runs for $L = 30, 40, 50$, and 100 runs for $L = 10\,000$. The dotted line corresponds to $\beta = 0.25$.

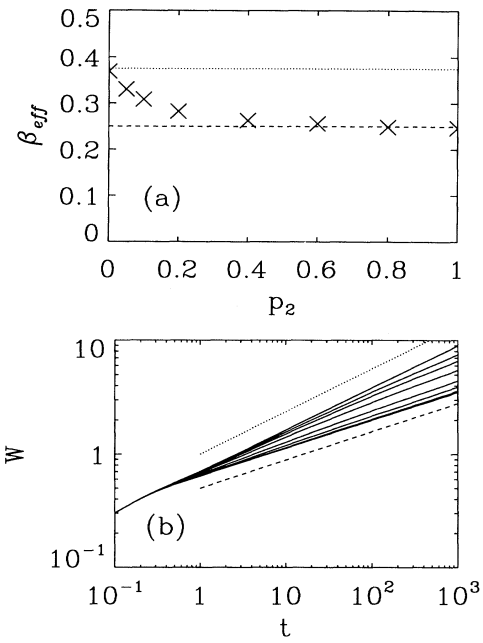

FIG. 13. (a) The calculated effective exponent $\beta_{\rm eff}$ as a function of the probability p_2 in model 2. The diffusion probability $p_1 = 1$ and the diffusion length $\ell = 1$. The dotted line corresponds to $\beta = 0.375$ and the dashed line to $\beta = 0.25$. (b) The calculated width W as a function of growth time t in the new model for various values of the probability p_2 of breaking two bonds, used to calculate $\beta_{\rm eff}$ given in (a). The system size $L = 10\,000$ and the number of runs is 100. The effective exponents are the slope of the curves in the highest decade. The dotted line corresponds to $\beta = 0.375$ and the dashed line to $\beta = 0.25$.

$p_1 = 1$. Again, the crossover from ~ 1.3 (KD) to 0.5 (RDR) is evident from this figure. In Fig. 14(b) we show the interface width W as a function of time t for some values of the probability p_2. In Fig. 14(c) we show the $\ln(W_{\rm sat})$ versus $\ln(L)$ curves whose slopes give $\alpha_{\rm eff}$ for the different values of p_2.

We believe that, given the similarity of the diffusion mechanisms defined in each of our models, the data just shown suggest that a similar crossover (from KD to RDR) may occur in model 1 when the temperature becomes large. The fact that we did not observe this crossover in Sec. II is due, we think, to finite-size effects, which completely mask the RDR scaling at high temperatures. Thus high-temperature MBE (without any overhangs and vacancies) may actually belong to EW universality with the intermediate-temperature behavior dominated by KD universality.

D. Scaling

In Fig. 15 we show the calculated scaling function for model 2, $W(L,t)/L^{\alpha_{\rm eff}}$ as a function of $t/L^{z_{\rm eff}}$, as discussed in Sec. II C in the context of model 1. In Figs. 15(a) and 15(b) we give results for the case $p_2 = 0$, i.e., the KD model without two-bond-breaking hops. No-

tice that we rescale time and width using effective exponents rather than asymptotic ones. Figure 15(c) corresponds to $p_2 = 1$, where model 2 has crossed over to the RDR-EW universality class, as can be seen from the values of the exponents used to rescale time and width. Basically the considerations made about the scaling function for model 1 apply in this case as well.

IV. DISCUSSION

A. Morphologies

In Figs. 16(a)–16(h) we show the surface morphologies produced by model 1 at different temperatures. All of these surface morphologies are in the steady-state saturation regime, where the interface width becomes time independent. The roughness of these morphologies is then the maximum possible roughness that can be achieved at each temperature. Notice that since the onset of saturation depends on the temperature, the average height of the deposits (taken as the origin of coordinates) is not the same for the different temperatures. The most striking feature of the morphology at low temperatures is the formation of deep and narrow valleys, which are smoothed out at higher temperatures. This jagged and extremely rough morphology is a consequence of the large value of $\alpha_{\rm eff}$ in the 1D MBE model.

In Figs. 17(a)–17(e) we see that the same kind of structures appear in model 2 for $p_2 = 0$, and therefore we conclude that the formation of deep valleys surrounded

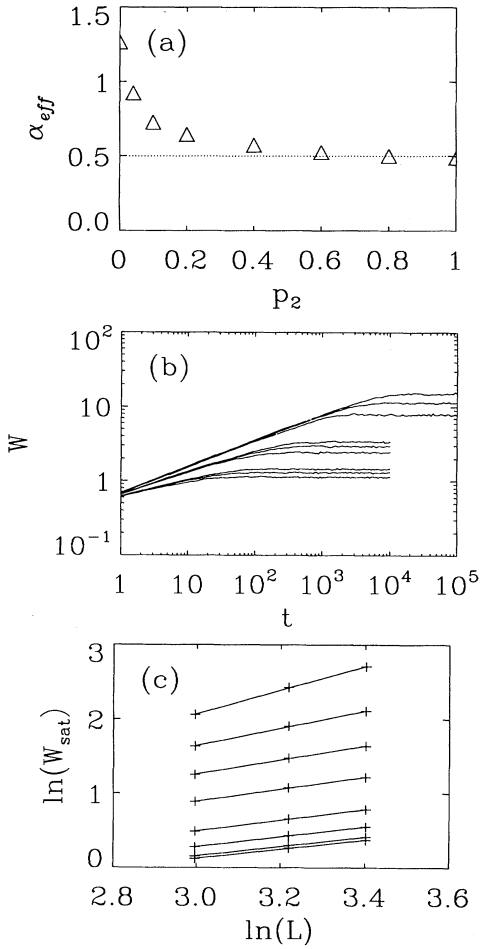

FIG. 14. (a) The effective exponent $\alpha_{\rm eff}$ as a function of the probability p_2 in model 2. The diffusion probability $p_1 = 1$ and the diffusion length $\ell = 1$. (b) Interface width W as a function of time t. The saturation regime data from curves like these was used to obtain $\alpha_{\rm eff}$. From top to bottom, groups of three curves correspond to the system sizes $L =$ 50,40,30, for the probabilities $p_2 = 0$, 0.1, and 1. Results are averaged over 1000 runs. (c) Logarithm of the saturation width $W_{\rm sat}$ vs logarithm of the system size L, for different values of the probability p_2. The straight lines are linear fits to the calculated saturation widths and their slopes are the effective exponents $\alpha_{\rm eff}$. From top to bottom, the curves correspond to $p_2 = 0, 0.04, 0.1, 0.2, 0.4, 0.6, 0.8, 1$.

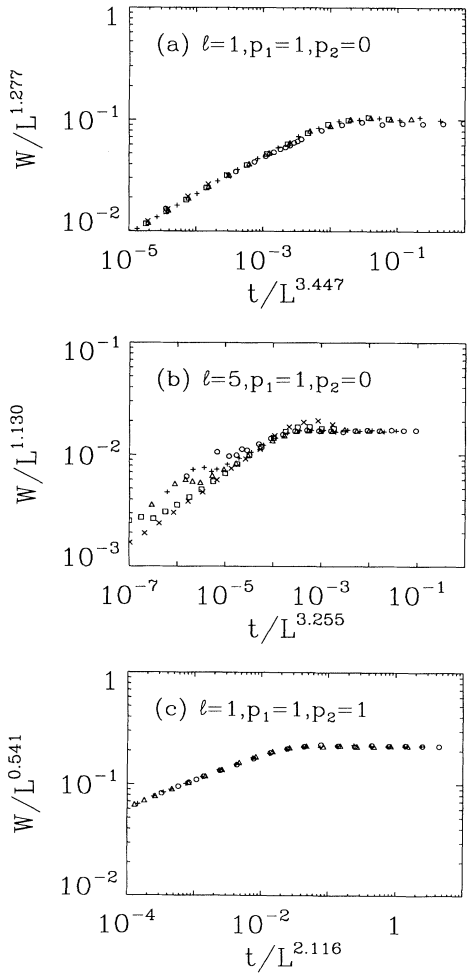

FIG. 15. Scaling function $f(t/L^{\alpha_{\rm eff}/\beta_{\rm eff}}) = W/L^{\alpha_{\rm eff}}$ as obtained from the simulation in model 2. The figure shows the collapse of the data into the scaling function form for different system sizes: (a) $\ell = 1$, $p_1 = 1$, $p_2 = 0$, $L = 10$ (circles), 30 (pluses), 40 (triangles), 50 (squares), and 64 (crosses); (b) $\ell = 5$, $p_1 = 1$, $p_2 = 0$, $L = 30$ (circles), 40 (pluses), 50 (triangles), 100 (squares), and 200 (crosses); (c) $\ell = 1$, $p_1 = 1$, $p_2 = 1$, $L = 30$ (circles), 40 (pluses), 50 (triangles).

by high steps is due to the migration of surface atoms to nearby kink sites. We verify that longer diffusion lengths ℓ produce locally smoother surfaces and smaller typical step heights, corresponding to high temperatures in the first model. This local smoothness at length scales comparable to the system size causes the effective exponents to approach zero or, in other words, the asymptotic scaling exponents can only be calculated using system sizes much larger than the typical length scales of the surface fluctuations. In Figs. 17(f) and 17(g) we show surface morphologies produced with $p_2 = 1$, which corresponds, as discussed above, to the RDR model. Comparing Figs. 17(a) and 17(f), which differ only in the value of p_2 (0 and 1), we clearly see that the high steps characteristic of the KD model disappear when two-bond-cutting processes are allowed. Since the presence of high steps naturally leads to overhangs and bulk vacancies, the activation of two-bond-cutting diffusion at high temperatures in MBE growth is important to avoid those defects.

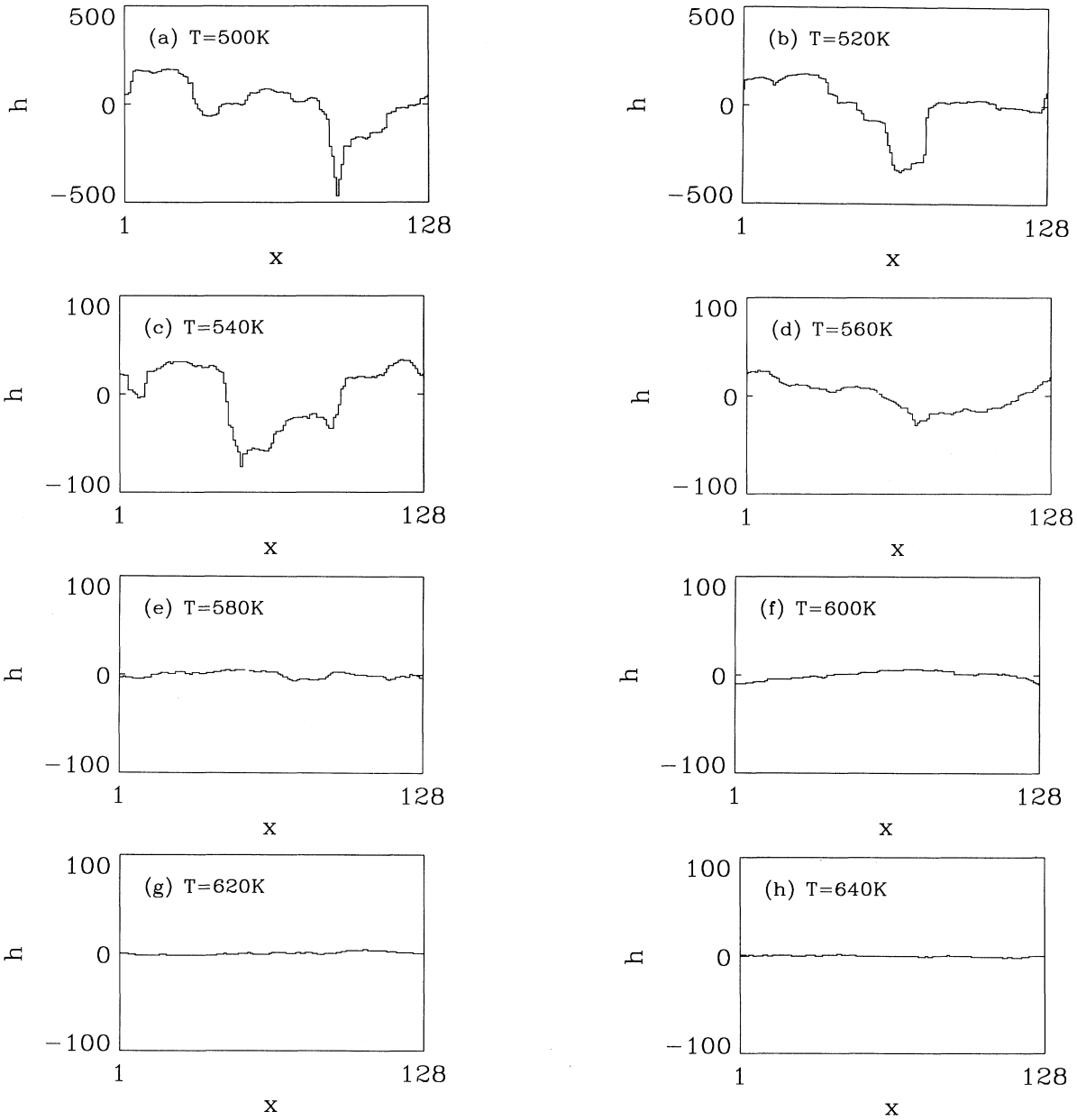

FIG. 16. Surface morphologies in model 1 in the saturation regime for (a) $T = 500$ K, (b) $T = 520$ K, (c) $T = 540$ K, (d) $T = 560$ K, (e) $T = 580$ K, (f) $T = 600$ K, (g) $T = 620$ K, and (h) $T = 640$ K. We plot the height h of the deposit as a function of the substrate site x, with the origin of the h axis shifted by the average height to show only the surface. Notice that the range of the h axis is larger for $T = 500$ and 520 K than for the other temperatures.

Is the SOS model a realistic approximation to the real MBE growth, or must overhangs and vacancies be considered in the simulations? Overhangs are important only when high steps tend to develop as, for example, happens in model 1 at low temperature; in this case, allowing overhangs is a realistic choice which would lead to vacancies in the bulk and smoother surfaces. In fact, this is just the ballistic deposition model which belongs to the KPZ universality class ($\beta = 1/3$, $\alpha = 1/2$). At $T = 600$ K the high steps have been almost completely eliminated and, at higher temperatures, steps higher than one lattice spacing are unlikely. Thus, in the high-temperature limit, allowing overhangs should not affect the surface morphology substantially and, moreover, we expect that

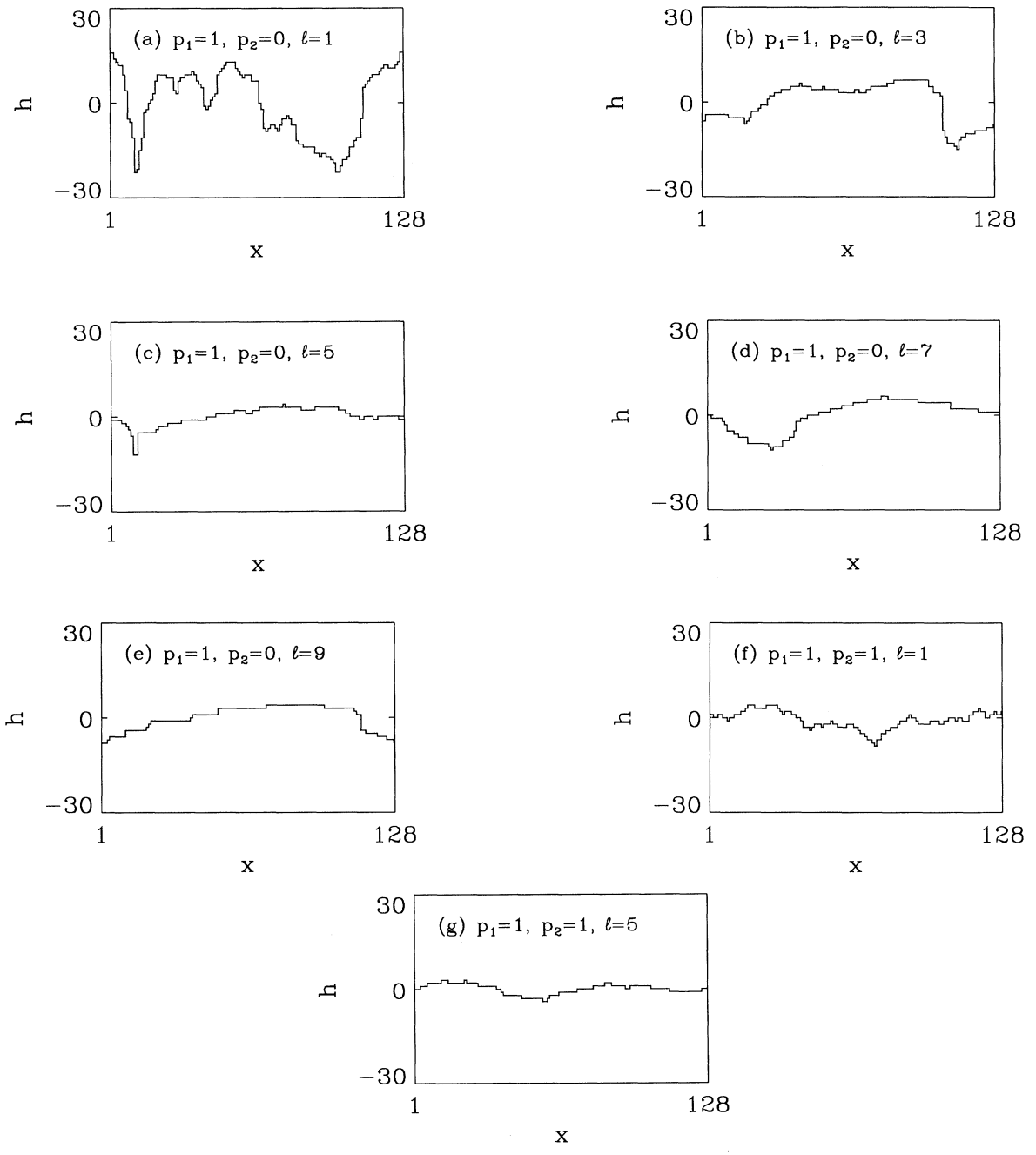

FIG. 17. Surface morphologies in model 2 in the saturation regime for $p_1 = 1$ and (a) $p_2 = 0$, $\ell = 1$, (b) $p_2 = 0$, $\ell = 3$, (c) $p_2 = 0$, $\ell = 5$, (d) $p_2 = 0$, $\ell = 7$, (e) $p_2 = 0$, $\ell = 9$, (f) $p_2 = 1$, $\ell = 1$, and (g) $p_2 = 1$, $\ell = 5$. We plot the height h of the deposit as a function of the substrate site x, with the origin of the h axis shifted by the average height to show only the surface.

EW (not KPZ) will still be the universality class of the model, except for unphysically large system sizes where the asymptotic KPZ critical behavior may show up.

B. Finite-size effects

The scaling relations Eqs. (2) and (3) are valid in the limit of large times and system sizes. (In fact, the basis for the dynamic scaling hypothesis is that L and t are the only relevant length and time scales in the problem.) In this limit, the scaling exponents β and α are universal in the sense that they are independent of the parameters of the models. For finite systems and times, we handled the corrections to scaling by introducing effective exponents $\beta_{\rm eff}$ and $\alpha_{\rm eff}$ such that $W \sim t^{\beta_{\rm eff}}$ and $W_{\rm sat} \sim L^{\alpha_{\rm eff}}$, which are no longer universal. The relevant parameters on which the effective exponents depend are the temperature T (which determines the hopping rates R_1 and R_2), the deposition rate R_d, and the system size L. However, it may be more useful to express that dependence in terms of L and some diffusion length, suitably defined in terms of T and R_d.

A number of definitions of a surface diffusion length $\mathcal{L}$ have been introduced, and its dependence on the deposition time $\tau \equiv 1/R_d$ and the diffusion constant ν_1 [following the notation of Eq. (A7)] has been estimated to be of the form $\mathcal{L}^\gamma \sim \nu_1 \tau$. For the exponent γ, de Miguel *et al.* [18], Irisawa *et al.* [19], and Das Sarma, Lai, and Tamborenea [20] proposed that $\gamma = d + 1$, and Stoyanov [21] and Villain [22], suggested $\gamma = d + 3$. Recently, Ghaisas and Das Sarma have considered this question in details [23]. Although we consider that it may be simplistic to describe real MBE growth using a single diffusion length parameter $\mathcal{L}$, here we present a finite-size analysis using a diffusion length as the relevant parameter.

According to the analytical treatment of the Eq. (A7) by Das Sarma, Lai, and Tamborenea [20], the interface width W, and hence the effective exponent $\beta_{\rm eff}$, depends on the parameter $\nu_1 \tau / L^4$. Using the estimate $\mathcal{L}^\gamma \sim \nu_1 \tau$, the dependence of $\beta_{\rm eff}$ on $\mathcal{L}$ and L becomes of the form $\beta_{\rm eff} = \beta_{\rm eff}(\mathcal{L}^\gamma / L^4)$. If we now refer to the KD model (our model 2 with $p_2 = 0$), whose asymptotic exponents are close to those of the linear gradient fourth equation [Eq. (A7)], we can identify the physical diffusion length $\mathcal{L}$ with the parameter ℓ of the model and use the simulation results to see whether $\gamma = 3$ or 5 (for $d = 2$) gives the best data collapse to a unique $\beta_{\rm eff}(\mathcal{L}^\gamma / L^4)$ expression. In Figs. 18(a) and 18(b) we plot $\beta_{\rm eff}$ as a function of ℓ^γ / L^4, for $\gamma = 3$ and 5, respectively, for various values of the diffusion length ℓ. For comparison, we also give $\beta_{\rm eff}$ as a function of ℓ^4 / L^4 in Fig. 18(c). Clearly, a larger value of γ rescales the data in the right direction and therefore we conclude that our results are more consistent with $\gamma = 5$ than with $\gamma = 3$. This finite-size analysis should be taken with caution since the data collapse that it produces is not completely satisfactory and it relies on many assumptions that may turn out to be too simplistic. In particular, the assumption of a single $\mathcal{L}$ which has a unique power-law dependence on the deposition rate τ^{-1} is surely far too simplistic [23].

C. Sharp epitaxial temperature

To reconcile the experimental finding of a sharp epitaxial temperature [24] with the kinetic roughening concept, we argue that this discrepancy can be understood in terms of finite-size effects and the exponential dependence of the diffusion rates on the temperature. The fact that the surface roughness saturates to a time-independent value after a certain growth time (of the order of $L^{\alpha_{\rm eff}/\beta_{\rm eff}}$) can be used to give an operational definition of smooth growth and hence to determine the parameters T, R_d, and L such that smooth growth is achieved. For a given system size, the saturation width $W_{\rm sat}(T)$ is a decreasing function of the temperature, as shown in Fig. 19, for model 1. As a possible definition of smooth growth (in fact, a rather stringent one), we can demand the saturated width to be smaller than unity (these means that at all times the surface fluctuations will be smaller than one monolayer). We can then introduce an epitaxial temperature $T_e(L)$ separating our just defined rough and smooth regimes, such

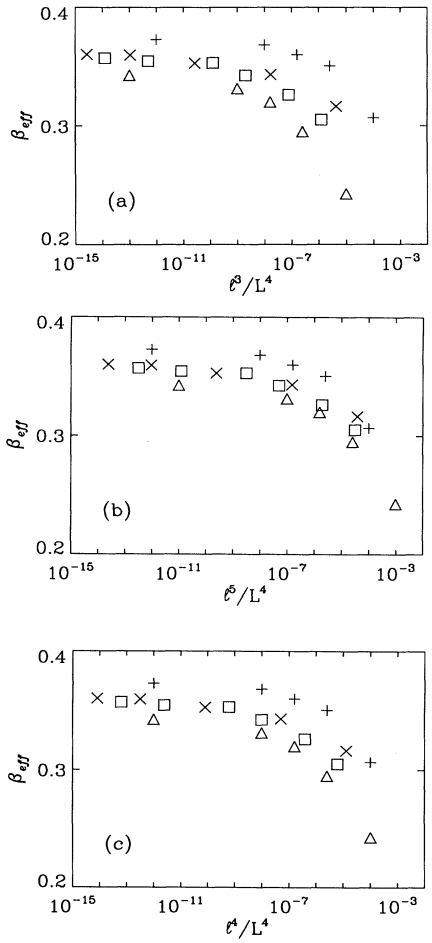

FIG. 18. The effective exponent $\beta_{\rm eff}$ in model 2, as a function of ℓ^γ / L^4, for different values of ℓ and γ: (a) $\gamma = 3$, (b) $\gamma = 5$, and (c) $\gamma = 4$. Pluses, crosses, squares, and triangles correspond to $\ell = 1$, 3, 5, and 10, respectively.

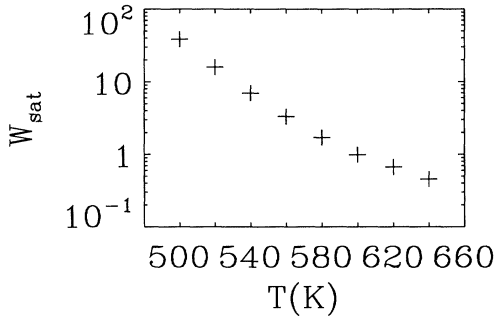

FIG. 19. The saturated width $W_{\rm sat}$ [$\equiv W(L, t \to \infty)$] as a function of the substrate temperature T in model 1, with $L = 30$.

that $W_{\rm sat}(L,T) \leq 1$ for $T \geq T_e(L)$. For example, in Fig. 19, $W_{\rm sat}(L = 30, T)$ becomes smaller than unity around $T_e \simeq 600$ K. We apply this procedure for different values of L and obtain the epitaxial temperature $T_e(L)$ as a function of the system size L. The result is shown as squares in Fig. 20. The important finding is that $T_e(L)$ basically saturates to a constant value for large L, which agrees with the experimentally well-known existence of a *sharp epitaxial temperature* separating rough and smooth growth. Note that the very weak dependence of T_e on L is a direct consequence of activated hopping diffusion.

A simple analytic argument based on the idea that smooth growth will be achieved when the diffusion length

$$\begin{aligned} \ell &= \sum_{n=1}^{2} \ell_n \\ &\approx \sum_{n=1}^{2} R_n^{1/2} \\ &= \sum_{n=1}^{2} \left(\frac{2k_B T}{h} e^{(E_0 + nW)/k_B T} \right)^{1/2} \end{aligned} \tag{7}$$

is comparable to the system size predicts a $T_e(L)$ given as triangles in Fig. 20. We can see that both simulation and a simple theory agree well with the experimental evidence of a sharp transition temperature. According to this idea, this relatively sharp transition is not a phase transition, but a consequence of the finite-size effects coupled with the exponential dependence of the diffusion rates on the temperature. The consequence of this exponential dependence is that large changes in L produce small (basically logarithmic) changes in T_e, and therefore T_e appears to be sharp, i.e., independent of L. We have recently [25] used this idea to qualitatively explain recent experimental findings of a critical epitaxial thickness in MBE growth [26].

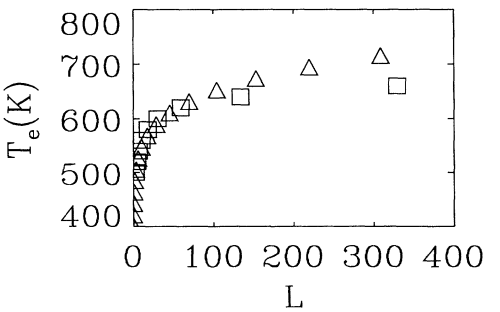

FIG. 20. Epitaxial temperature T_e as a function of the system size L. Squares give the simulation results in model 1, obtained by looking for the temperature at which the saturation width becomes smaller than unity for a given system size, and triangles correspond to the values calculated with a simple theory explained in the text.

D. Connection with continuum theories

The main goal of this paper is to present extensive atomistic simulation results for stochastically driven crystal growth in (1+1) dimensions under atomistic beam deposition process and to make connection with (one dimensional) MBE growth within a SOS, square-lattice model. But, throughout this article we have made appropriate references to various continuum growth equations (Appendix) which seem to describe well various numerically calculated growth exponents. In this subsection we summarize our findings in relation to various continuum models. An excellent discussion of this issue, from a somewhat complementary perspective, has recently been provided by Villain [27]. While our emphasis here is on atomistic simulations, Villain's theoretical approach is based on a long-wavelength macroscopic viewpoint. Lai and Das Sarma [15] have investigated this issue from a geometric-topological viewpoint and have provided a renormalization-group analysis of the nonlinear fourth-order equation [Eqs. (A8) and (A9)]. Das Sarma and Ghaisas [16] have recently investigated this issue in (2+1) dimensions via kinetic growth simulations.

We summarize our findings for the critical exponents in the two models (models 1 and 2).

Model 1

(1) At low temperatures, activated diffusion being negligible, we get $\beta_{\rm eff} = 1/2$ which corresponds to the random deposition case. Theoretically, this is obviously a finite-time effect in the simulation; however, diffusion being exponentially suppressed at low-temperatures, we expect our low-temperature results to hold in real growth situation, except that real growth will most likely crossover to KPZ universality because overhangs and vacancies will be generated in this extremely rough situation.

(2) At intermediate temperatures, activated hopping with the breaking of one bond becomes possible during the time scale of simulation (and also, we believe, during activated growth) and one gets crossover to the newly discovered KD universality class (which corresponds to atoms diffusing to kink sites) of our model 2 with $p_2 = 0$.

(3) At higher temperatures, crossover effects associated with the breaking of two bonds show up along with strong finite-size effects lowering both $\beta_{\rm eff}$ and $\alpha_{\rm eff}$. The effective exponents smoothly approach zero due to finite-

size effects associated with the diffusion length becoming larger than the system size.

(4) We believe that the universality class at high temperatures, where hopping diffusion with the breaking of two bonds becomes activated (but the temperature is *not* so high as to produce significant desorption), is the EW (or the RDR) where the atoms relax to the local height minima (as, for example, under a gravitational potential in the original EW paper). In our model, gravitation, of course, is totally negligible—but, in not allowing atoms to hop up, we are intrinsically assuming an attractive substrate (this is a physically well-valid assumption for MBE growth) which acts similar to a gravitational potential. In this situation, cutting of two bonds (i.e., only the lowest energy three-bond saturation is now stable) within the SOS model (i.e., no vacancies, overhangs, etc.) will clearly take atoms to local height minima mimicking EW growth (note that this is no longer true once desorption or bulk vacancy or overhang formation is allowed whence the EW universality will cross over to the ubiquitous KPZ universality, which probably does happen at still higher temperatures in MBE growth). We mention that absolutely unequivocal evidence for the higher-temperature crossover to EW universality is not obvious in our 1D MBE simulation because finite-size effects become important around where two-bond cutting processes are quantitatively significant.

The above points become self-evident once the simulation results of our model 2 are compared with those of model 1 in light of items (1)–(4) above.

Model 2

(1) In model 2, the situation $p_1 = p_2 \approx 0$ (or $\ll 1$) corresponds to the low-temperature 1D MBE growth (essentially no diffusion) of model 1. The growth process is then trivially RD producing $\beta_{\text{eff}} = 1/2$.

(2) Intermediate temperatures of model 1 correspond to $p_2 \approx 0$, but p_1 finite in model 2 so that there is significant diffusion to kink sites (but insignificant hopping *from* kink sites), which produces the KD universality of (according to our best estimates) $\beta = 0.371 \pm 0.005$ and $\alpha = 1.32 \pm 0.04$. This is, as noted before, intermediate between RD and RDR growth. This regime presumably corresponds to the linear fourth-order equation [Eq. (A7)] as was already noted earlier.

(3) For $\ell = 1$ and $p_1, p_2 \neq 0$ we get crossover effects in model 2 with competition among KD, EW, and finite-size effects. As p_2 (and ℓ) increases (equivalent to increasing temperature in model 1), finite-size effects produce substantial smoothing of the growing surface with the effective exponents approaching zero (similar to model 1).

(4) The high-temperature regime of model 1 corresponds to large values of p_2 in model 2. The result of increasing p_2 (keeping $p_1 \neq 0$) is, as we stated before, a crossover from the KD to the RDR-EW universality classes. Given the similarity between the diffusion mechanisms in both model, we conclude that model 1 would also show this crossover at high temperatures for large enough systems.

V. SUMMARY AND CONCLUSION

In this paper, we have presented a detailed numerical study of (1+1)-dimensional epitaxial growth within the square lattice, SOS model in the chemical bonding environment with an attractive substrate where the atomic deposition is purely random and the only allowed relaxation is surface diffusion via Arrhenius activated hopping. Bulk vacancy formation, overhangs, and desorption are not allowed, making the growth process conservative which rules out nonlinearities of the KPZ type (Appendix). We find this one-dimensional MBE growth model to satisfy the dynamic scaling hypothesis given by Eq. (1) and be dominated by crossover effects, among the RD, KD, and RDR universality classes—with RD and KD dominating at low and intermediate temperatures, respectively, and RDR-EW showing up weakly at higher temperatures as two-bond breaking events become operational. We also give detailed numerical results for a kinetic growth model which is a generalized version of the KD model introduced in Ref. [6]. Using system sizes of $L = 10^5$ and $L = 10^6$ we find the exponent β in the KD universality class to be $\beta = 0.371 \pm 0.005$ and our largest simulations give $\alpha = 1.32 \pm 0.04$. When two-bond-breaking hops are activated in this kinetic growth model we observe a crossover from KD to RDR universality.

We point out that our 1D MBE growth results may very well have some experimental relevance to situations involving atomic migrations on a vicinal substrate with steps. Our results, for example, apply directly to how the morphology of these steps evolves with time as new atoms migrate to the step edges. As such our 1D MBE simulation results should describe step evolution in the so-called step-flow MBE growth situation. If one can experimentally extract the growth exponents associated with the temporal roughening of the propagating steps (from, for example, time-resolved scanning tunnel microscope pictures taken during the step-flow MBE growth), one may be able to make a direct comparison with our theoretical predictions. Such an experimental evaluation of growth exponents via a statistical analysis of time-resolved STM pictures of steps has not yet been attempted, but should be useful in determining kinetic universality classes of growth with surface diffusion.

We note that any connection between our growth models and real MBE growth should be taken with caution, not only because our growth studies are in (1+1) dimensions but also because our models are based on certain assumptions which are currently a source of controversy. The main crititicism has to do with the asymmetry of the diffusion mechanisms: in our two models, the diffusion of atoms down a step or cliff is not limited by the height of the step, whereas the hops in the horizontal direction are nearest-neighbor hops in model 1, and are bounded by the parameter ℓ in model 2. These rules break the symmetry between horizontal and vertical diffusion and may lead to unphysically high steps in the surface morphology and probably to values of the exponent α larger than one. This is a valid criticism which has motivated recent work on kinetic growth simulations treating horizontal and vertical diffusion on an equal footing [28]. The result of this

treatment is essentially a recovery of the KPZ universality, as might have been anticipated, since the limitation on the velocity of vertical diffusion leads to overhangs and vacancies, which are typical of the BD model. We emphasize that theory, by itself, cannot settle the issue of the correct universality class for MBE growth; we must look at experiments for the answer. Very recent experimental results [29] in (2+1) dimensions are consistent with the LDS universality, and results for an equivalent physical system in (1+1) dimensions could produce exponents consistent with our KD universality, as discussed in the next paragraph. While more experimental results are clearly needed to settle this issue, our own viewpoint as emphasized here and in other publications [1, 16, 20, 30] is that real MBE growth will most likely be affected by crossover effects from RD, KD, and then, possibly, RDR-EW universalities as growth temperature (growth rate) increases (decreases), with the true asymptotic universality, which will be masked by strong finite-size effects, being the BD-KPZ universality. It may be appropriate to point out here that stochastic Arrhenius MBE growth simulations [17] have been quite successful in describing real MBE growth in (2+1) dimensions. In particular, "vertical" diffusion at very high steps is extremely rare in the actual simulations and may not be as severe a problem as it appears at first sight. Another aspect of our models that has raised criticism is the usage of a simple cubic geometry, and this problem has been addressed in Ref. [31].

Before we conclude, we briefly discuss why the simple linear model of Eq. (A7) involving the ∇^4 term seems to describe our intermediate temperature model 1 results or the $p_2 = 0$ version of model 2 results so well (i.e., $\beta \approx 0.375 = 3/8$ as it should be in both cases). This issue has been discussed recently by Lai and Das Sarma [15] from a geometrical-topological viewpoint. Here we note the curious fact that for our best simulations the asymptotic value of α seems to be more consistent with $\alpha \approx 1.32$ than with $\alpha = 1.5$ as the linear theory demands, even though the value of β seems to be 0.375 within our error bar ($\beta = 0.371 \pm 0.005$ according to our best simulations). There are three possibilities. One is that our calculated α has fairly large numerical errors (and the asymptotic α is indeed 1.5 as demanded by the linear theory) beyond our estimated statistical error bars. This is certainly possible since an accurate numerical determination of α from dynamical simulations is almost impossible. Another possibility is that the linear term $\nu\nabla^2 h$ is present in the continuum equation with a small but nonzero value of ν. This linear term would dominate over the ∇^4 term at long length scales, decreasing the exponent α from 1.5 to 0.5. It is clear, though, that our set of exponents (α, β) are much closer to those of Eq. (A7) than to the EW ones, which leads us to believe that the coefficient of a possible ∇^2 term, if this term is at all present in the underlying continuum equation, is much smaller than the coefficient of the ∇^4 term. The last possibility, which we cannot rule out, is that in our longest and largest simulations we are getting some nonlinear effects inherent in the atomistic kinetic simulation. We mention that the two mathematically and physically allowed nonlinear corrections to the ∇^4 [namely, the $\nabla^2(\nabla h)^2$ term and the $\nabla \cdot (\nabla h)^3$ term in Eq. (A9)] term are both relevant perturbations and reduce α from 1.5 to 1 and 0.75, respectively in $d = (1 + 1)$ dimensions (while affecting the value of β much less, changing it from 0.375 to 0.33 and 0.30, respectively—finite-size effects on β are also usually much smaller). Our simulation results rule out any dominant contributions from these nonlinear terms (i.e., their coefficients must be extremely small) in finite-size samples, but these perturbations being relevant (in the dynamical renormalization-group sense) the asymptotic exponents should be determined by these nonlinearities. Unfortunately, in spite of considerable effort, we are unable to decisively resolve this issue because numerical extraction of an unambiguous asymptotic α from stochastic simulation for our model, where $z_{\text{eff}} \approx 4$ making $\tau \sim L^4$, is essentially impossible. Further work is needed in this direction because, as has been noted by a number of authors, $\alpha > 1$ is physically unacceptable in the thermodynamic limit. It would imply that the surface width fluctuations, $W_{\text{sat}} \sim L^{\alpha}$, will exceed the lateral system size for a large enough sample, clearly indicating a highly unstable situation. Any infinitesimal nonlinearity will then completely dominate the asymptotic growth dynamics. The problem is not as severe as it sounds in real systems because typically $W_{\text{sat}} \ll L$ even for fairly large values of L. But, we clearly have a theoretical, conceptual problem that needs to be resolved. We emphasize that no such problem arises in (2+1)-dimensional simulations [16, 32] where the fourth order nonlinearities seem to manifest themselves in all their glory. The reason for the absence of nonlinear corrections (or, at least, of an extremely slow crossover) to the critical exponents in (1+1)-dimensional epitaxial growth simulations remains a mystery.

ACKNOWLEDGMENTS

This work is supported by the United States Office of Naval Research and the National Science Foundation.

APPENDIX

In this appendix we present several continuum models which have been proposed to describe dynamic growth. We intend to summarize here, without any real derivations, the mathematical aspects of the different growth models to complement the numerical simulation and the physical discussion given in the text. We consider a surface growing on a flat substrate, and denote by $h(\mathbf{x}, t)$ the height of the surface at time t above the substrate site $\mathbf{x}$. The dimension of the substrate is $d' = d - 1$. We assume that $h(\mathbf{x}, t)$ is a single-valued function of $\mathbf{x}$ and its time evolution is governed by an equation of the form

$$\frac{\partial h}{\partial t} = \lambda_0 + \nu\nabla^2 h - \nu_1\nabla^4 h + \lambda(\boldsymbol{\nabla} h)^2 + \lambda_1\nabla^2(\nabla h)^2 + \lambda_2\boldsymbol{\nabla}\cdot(\boldsymbol{\nabla} h)^3 + \lambda_3(\nabla^2 h)^2 + \cdots + \eta \qquad \text{(A1)}$$

where all terms up to fourth order which are consistent with the symmetry of the problem have been kept and η is

the stochastic noise associated with the incident particle beam, usually taken to have a Gaussian distribution with

$$\langle \eta \rangle = 0, \tag{A2}$$

$$\langle \eta(1)\eta(2) \rangle = 2D\delta^{d'}(\mathbf{x}_1 - \mathbf{x}_2)\delta(t_1 - t_2). \tag{A3}$$

The constant velocity term λ_0 associated with the average deposition rate can be removed by choosing an appropriate moving coordinate system. A geometrical interpretation of the different terms in Eq. (A1) is attempted in Ref. [15] by Lai and Das Sarma. Here the noise is assumed to be uncorrelated, but continuous models of interface growth with correlated noise have also been studied [33]. If the growth process is conservative, i.e., a mass conservation law is obeyed, the growth equation must obey a continuity equation

$$\frac{\partial h}{\partial t} = -\boldsymbol{\nabla} \cdot \mathbf{j} + \eta, \tag{A4}$$

where $\mathbf{j}$ is a surface current perpendicular to the growth direction. This form disallows terms such as $\lambda(\boldsymbol{\nabla} h)^2$ and $\lambda_3(\nabla^2 h)^2$ in Eq. (A1), and, in particular, the model by Kardar, Parisi, and Zhang [8]

$$\frac{\partial h}{\partial t} = \nu \nabla^2 h + \lambda(\boldsymbol{\nabla} h)^2 + \eta \tag{A5}$$

is ruled out if this conservation law is enforced. The scaling exponents for the KPZ equation are in (1+1) dimensions, $\beta = 1/3$ and $\alpha = 1/2$. In (2+1) dimensions, a numerical integration of the KPZ equation [34] gives $\beta \approx 0.25$ and $\alpha \approx 0.38$ (in the strong-coupling limit $\lambda \to \infty$) in agreement with simulations of discrete microscopic models, $\beta \approx 0.24$–0.25, $\alpha \approx 0.38$–0.4. See Refs. [2, 4] for further references on the KPZ equation and related atomistic models. Typically, overhangs (which lead to vacancies) and desorption are the mechanisms that break the mass conservation law. In "good" MBE growth, vacancies and overhangs are not allowed and usually there is very little desorption. Thus MBE growth may very well be an example of conservative growth.

The Edwards-Wilkinson equation corresponds to keeping only the lowest-order linear term in Eq. (A1):

$$\frac{\partial h}{\partial t} = \nu \nabla^2 h + \eta. \tag{A6}$$

This linear equation can be solved by Fourier transformation, and the growth exponents are, in d dimensions, $\beta = (3-d)/4$ and $\alpha = (3-d)/2$. The only relevant higher-order term that changes the universal scaling properties of the EW model is the KPZ nonlinearity $(\boldsymbol{\nabla} h)^2$. Recently, it was suggested [5, 6, 15] that the linear equation, which has $\beta = (5-d)/8$ and $\alpha = (5-d)/2$ with $z = 4$ given by

$$\frac{\partial h}{\partial t} = -\nu_1 \nabla^4 h + \eta, \tag{A7}$$

may be closely related to MBE growth at intermediate temperatures. Our numerical simulation with model 2 with $p_2 = 0$ indicates that, in (1+1) dimensions, $\beta = 0.371 \pm 0.005$ and $\alpha = 1.32 \pm 0.04$ ($z = 3.6$). Wolf and Villain [5] find $\beta = 0.365 \pm 0.015$ and $\alpha = 1.4 \pm 0.1$ ($z = 3.8 \pm 0.5$).

Lai and Das Sarma [15] proposed the nonlinear equation

$$\frac{\partial h}{\partial t} = -\nu_1 \nabla^4 h + \lambda_1 \nabla^2 (\boldsymbol{\nabla} h)^2 + \eta \tag{A8}$$

as being relevant to MBE growth. The term $\lambda_1 \nabla^2 (\boldsymbol{\nabla} h)^2$ is a relevant correction to the $\nu_1 \nabla^4 h$ term and changes the growth exponents, rendering a physically more acceptable value of α in (1+1) and (2+1) dimensions. Using perturbative renormalization-group technique, they find $\beta = (5-d)/(7+d)$ and $\alpha = (5-d)/3$ [$z = (7+d)/3$]. Sun, Guo, and Grant [35] studied a similar equation but with a *conserved* noise and obtained, in (1+1) dimensions, $\beta = 1/11$ and $\alpha = 1/3$ ($z = 11/3$).

The most general *conserved* equation (up to fourth order) is, however, given by

$$\frac{\partial h}{\partial t} = \nu \nabla^2 h - \nu_1 \nabla^4 h + \lambda_1 \nabla^2 (\boldsymbol{\nabla} h)^2 + \lambda_2 \boldsymbol{\nabla} \cdot (\boldsymbol{\nabla} h)^3 + \eta \tag{A9}$$

which contains the EW relaxation term $\nu \nabla^2 h$. Clearly, the $\nu \nabla^2 h$ term dominates the asymptotic scaling properties of this equation even though there may be strong crossover effects arising from the higher-order terms. It is fair to say that at the present time we do not know which of these continuum equations, if any, applies to the epitaxial growth problem. Another possible candidate is Eq. (A9) with $\lambda_2 = 0$ (whose asymptotic property is again dominated by the EW universality). The dynamical critical exponents corresponding to each of the terms in Eq. (A9) are known. [The $\lambda_2 \boldsymbol{\nabla} (\boldsymbol{\nabla} h)^3$ nonlinearity was also solved by Lai and Das Sarma [15] to obtain $\beta = (5-d)/2(3+d)$, $\alpha = (5-d)/4$, and $z = (3+d)/2$.]

We conclude this appendix by mentioning that one "popular" choice for the conserved equation describing epitaxial growth with no desorption, overhangs, or vacancies seems to be our Eq. (A9) with $\lambda_2 = 0$:

$$\frac{\partial h}{\partial t} = \nu \nabla^2 h - \nu_1 \nabla^4 h + \lambda_1 \nabla^2 (\boldsymbol{\nabla} h)^2 + \eta. \tag{A10}$$

Asymptotic critical properties of this equation are obviously the same as those of the EW equation, but there may very well be strong crossover effects arising from the fourth-order terms. Our (1+1)-dimensional simulations for 1D MBE growth process as presented in this paper are consistent with Eq. (A10) with the following caveats about finite-size and crossover effects: (i) at "low" temperatures, $\nu \approx \nu_1 \approx \lambda_1 \approx 0$; (ii) at "intermediate" temperatures, $\nu_1 \gg \nu, \lambda_1 \approx 0$; and (iii) at "high" temperatures, $\nu \neq 0$.

[1] F. Family, Physica A **168**, 561 (1990); S. Das Sarma, J. Vac. Sci. Tech. B **10**, 1695 (1992).
[2] J. Krug and H. Spohn, in *Solids far from Equilibrium: Growth, Morphology and Defects*, edited by C. Godriche (Cambridge University Press, Cambridge, 1990).
[3] T. Vicsek, *Fractal Growth Phenomena* (World Scientific, Singapore, 1989).
[4] *Dynamics of Fractal Surfaces*, edited by F. Family and T. Vicsek (World Scientific, Singapore, 1991).
[5] D. Wolf and J. Villain, Europhys. Lett. **13**, 389 (1990).
[6] S. Das Sarma and P. Tamborenea, Phys. Rev. Lett. **66** 325, (1991).
[7] E. F. Edwards and D. R. Wilkinson, Proc. R. Soc. London Ser. A **381**, 17 (1982).
[8] M. Kardar, G. Parisi, and Y. Zhang, Phys. Rev. Lett. **56**, 889 (1986).
[9] F. Family and T. Vicsek, J. Phys. A **18**, L75 (1985).
[10] F. Family, J. Phys. A **19**, L441 (1986).
[11] P. Meakin and R. Jullien, J. Phys. (Paris) **48**, 1651 (1987); R. Jullien and P. Meakin, Europhys. Lett. **4**, 1385 (1987).
[12] M. J. Vold, J. Colloid Sci. **14**, 168 (1959); P. Ramanlal and L. M. Sanders, Phys. Rev. Lett. **54**, 2289 (1985); P. Meakin, P. Ramanlal, L. M. Sanders, and R. C. Ball, Phys. Rev. A **34**, 5091 (1986).
[13] C. Herring, in *The Physics of Powder Metallurgy*, edited by W. E. Kingston (McGraw-Hill, New York, 1951); W. W. Mullins, J. Appl. Phys. **28**, 333 (1957); **30**, 77 (1959); P. Nozieres, J. Phys. (Paris) **48**, 1605 (1987).
[14] J. M. Kim and J. M. Kosterlitz, Phys. Rev. Lett. **62**, 2289 (1989).
[15] Z.-W. Lai and S. Das Sarma, Phys. Rev. Lett. **66**, 2348 (1991).
[16] S. Das Sarma and S. V. Ghaisas, Phys. Rev. Lett. **69**, 3762 (1992).
[17] S. Das Sarma, J. Vac. Sci. Tech. A **8**, 2714 (1990), and references therein; S. Das Sarma, I. K. Marmorkos, and S. M. Paik, Surf. Sci. **228**, 28 (1990); I. K. Marmorkos and S. Das Sarma, Surf. Sci. Lett. **237**, L411 (1990); Phys. Rev. B **45**, 11262 (1992).
[18] J. J. de Miguel *et al.*, Surface Sci. **189/190**, 1062, (1987); see also J. Cryst. Growth **88**, 442 (1988); and **91**, 481 (1988).
[19] T. Irisawa *et al.*, J. Cryst. Growth **99**, 491 (1990).
[20] S. Das Sarma, Z. W. Lai, and P. I. Tamborenea, Surf. Sci. Lett. **268**, L311 (1992).
[21] S. Stoyanov, Surf. Sci. **199**, 226, (1988).
[22] J. Villain (unpublished).
[23] S. V. Ghaisas and S. Das Sarma, Phys. Rev. B **46**, 7308 (1992).
[24] R. T. Tung and F. Schrey, Phys. Rev. Lett. **63**, 1277 (1989); J. H. Neave *et al.*, Appl. Phys. Lett. **47**, 100 (1985); H. Jorke, H. -J. Herzog, and H. Kibbel, Phys. Rev. B **40**, 2005 (1989); E. Chason *et al.*, J. Vac. Sci. Tech. B **7**, 332 (1989); E. Kasper and H. Jorke, in *Chemistry and Physics of Solid Surfaces*, edited by R. Vanselow and R. Howe (Springer-Verlag, Berlin, 1988), p. 557.
[25] S. Das Sarma and P. I. Tamborenea, Phys. Rev. B **46**, 1925 (1992).
[26] D. J. Eaglesham, H. -J. Grossmann, and M. Cerullo, Phys. Rev. Lett. **65**, 1227 (1990).
[27] J. Villain, J. Phys. I **1**, 19 (1991).
[28] H. Yan, Phys. Rev. Lett. **68**, 3048 (1992); D. A. Kessler, H. Levine, and L. M. Sander, *ibid.* **69**, 100 (1992); C. J. Lanczycki and S. Das Sarma (unpublished).
[29] Y.-L. He, H.-N. Yang, T.-M. Lu, and G.-C. Wang, Phys. Rev. Lett. **69**, 3770 (1992).
[30] P. I. Tamborenea, Z. W. Lai, and S. Das Sarma, Surf. Sci. **267**, 1 (1992).
[31] H. C. Kang and J. W. Evans, Surf. Sci. **271**, 321 (1992).
[32] M. Kotrla, A. C. Levi, and P. Smilauer, Europhys. Lett. **20**, 25 (1990); M. R. Wilby, D. D. Vvedensky, and A. Zangwill, Phys. Rev. B **46**, 12 896 (1992).
[33] E. Medina, T. Hwa, M. Kardar, and Y.-C. Zhang, Phys. Rev. A **39**, 3053 (1989).
[34] Jacques G. Amar and Fereydoon Family, Phys. Rev. A **41**, 3399 (1990).
[35] Tao Sun, Hong Guo, and Martin Grant, Phys. Rev. A **40**, 7673 (1989).